Engineering Geology 121 (2011) 28–45

Contents lists available at ScienceDirect

Engineering Geology

journal homepage: www.elsevier.com/locate/enggeo

Large-scale subaerial and submarine Holocene and recent mass movements in the Betsiamites area, Quebec, Canada

Geneviève Cauchon-Voyer [a,*], Jacques Locat [a], Serge Leroueil [b], Guillaume St-Onge [c,d], Denis Demers [e]

[a] Université Laval, Département de géologie et génie géologique, Québec, Québec, Canada G1K 7P4
[b] Université Laval, Département de génie civil, Québec, Québec, Canada G1K 7P4
[c] Canada Research Chair in Marine Geology, ISMER, Université du Québec à Rimouski, Rimouski, Québec, Canada G5L 3A1
[d] Centre de recherche en géochimie et géodynamique (GEOTOP), Université du Québec à Montréal, C.P. 8888, Succ. Centre-Ville, Montréal, Québec, Canada H3C 3P8
[e] Ministère des Transports du Québec, Service géotechnique et géologie, 930, chemin Sainte-Foy, 5ème étage, Québec, QC, Canada G1S 4X9

ARTICLE INFO

Article history:
Received 13 August 2010
Received in revised form 5 April 2011
Accepted 8 April 2011
Available online 22 April 2011

Keywords:
Flowslide
Lateral spread
Sensitive clay
Submarine mass movements
Earthquakes
St. Lawrence estuary

ABSTRACT

At least three major landslide events formed the submarine and subaerial Betsiamites (Québec, Canada) landslide complex and mobilized an estimated total volume of 2000 million m^3 (2 km^3). Linkage between offshore and onshore geophysical investigations with borehole data and in situ testing allows reconstruction of the architecture of the Betsiamites River delta area and leads to the identification of the main failure events. The submarine scar of the Betsiamites landslide complex may have resulted from a first failure, dated at about 9250 cal BP, which mobilized a minimum volume of 200 million m^3. A second landslide dated at 7250 cal BP mobilized a volume of 1300 million m^3 over an area of 54 km^2. The Betsiamites submarine landslide event dated at 7250 cal BP left the largest scar yet identified on the St. Lawrence estuary seafloor. Furthermore, this paper demonstrates that the subaerial scar of the Betsiamites landslide complex is a result of the Colombier landslide event, which was initiated by the 1663 earthquake and involved four successive failure phases: one submarine and three subaerial. The February 5th 1663 earthquake triggered a submarine landslide event, which reached the shoreline, and led in a short period of time successively to two subaerial flowslides in sensitive clayey material and a subaerial lateral spread. The four failure phases mobilized a possible total volume of about 530 million m^3 over an area of 20 km^2. The Colombier landslide event is among the largest documented historic landslides in Canada. The presence of submarine scars left by the early Holocene events acted as predisposition factors for the development of the failure while the earthquake of 1663 was the main triggering factor of the first submarine failure.

1. Introduction

Human development and activities tend to occur along the coast, which justifies the relevance of studying coastal geologic hazards. In Eastern Canada (Figure 1), along the St. Lawrence estuary, part of the coastline is interrupted by large deltaic complexes. These deltaic sediments were deposited in post-glacial seas where many regressive deltas were constructed in a time of falling relative sea-level (e.g., Hart and Long, 1996). A rapid lowering of relative sea-level in conjunction with high sedimentation rates can create metastable slopes prone to mass movements (e.g., Sultan et al., 2004) and such conditions are frequently met in post-glacial deltaic environments (McKenna et al., 1992; Christian et al., 1997).

Scars of such failures are present in the lifted and submerged Quaternary sediments of the Betsiamites River delta area, on the North Shore region of the Province of Quebec, Canada (Figure 1), close to the municipality of Colombier and about 400 km north-east of Quebec City. The Betsiamites landslide complex is the result of separate subaerial and submarine failure events (Bernatchez, 2003; Cauchon-Voyer et al., 2008). The Colombier subaerial landslide scar, which is the subaerial part of the Betsiamites landslide complex, was first studied by Bernatchez (2003) who suggested, following aerial photo interpretation, that the scar may have resulted from at least two distinct failure events. Radiocarbon dating of a tree trunk and a marine shell allowed suggestion that both associated failures were triggered simultaneously by a strong earthquake (M~7) (Bernatchez, 2003) that occurred in the Province of Québec on February 5th, 1663 (Smith, 1962; Locat, in press). This age estimation for the subaerial landslide is additionally supported by historical account of landslide events in the Betsiamites area (Thwaites, 1959) and by dating, through ^{210}Pb derived sedimentation rates, of subaerial debris deposited offshore (Cauchon-Voyer et al., 2008). With an estimated area of 9.6 km^2 and more than 385 hm^3 (1 cubic hectometer = 1 million m^3) of mobilized material, the Colombier subaerial scar is likely to be one of the largest known to have occurred in the province of Quebec, comparable to the 1663 St-Jean Vianney subaerial landslide (e.g., Lasalle and Chagnon, 1968; Potvin et al., 2001).

* Corresponding author. Tel.: +1 418 656 2131x8604; fax: +1 418 656 7339.
E-mail address: genevieve.cauchon-voyer.1@ulaval.ca (G. Cauchon-Voyer).

0013-7952/$ – see front matter © 2011 Elsevier B.V. All rights reserved.
doi:10.1016/j.enggeo.2011.04.011

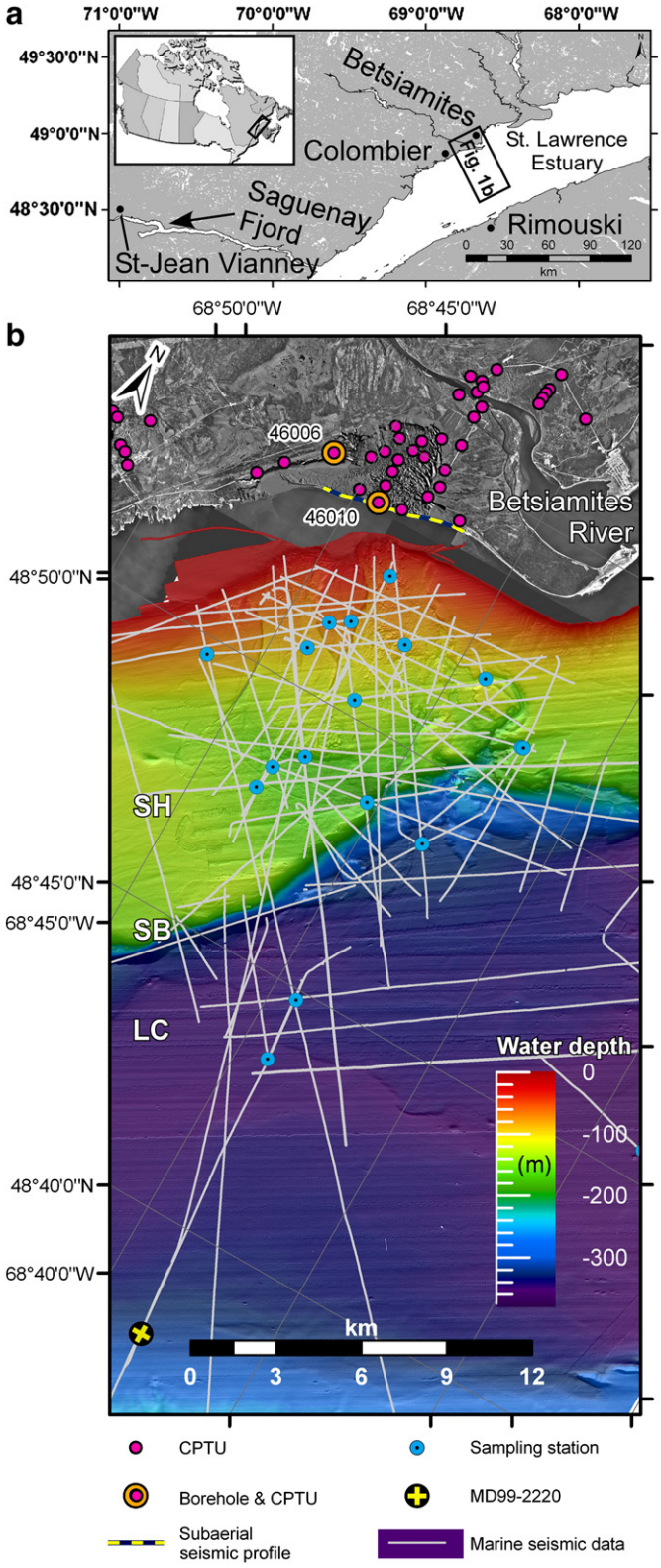

Fig. 1. Study site. a) Map of the St. Lawrence estuary in Canada with the locations discussed in this paper; b) subaerial and submarine investigations with location of the geophysical data, boreholes, marine sediments cores, and CPTUs. Shelf (SH), shelf break (SB) and Laurentian Channel (LC). The sampling location of core MD99-2220 is also illustrated. Map layout is rotated by 30°.

In addition to the Colombier subaerial scar, the adjacent submarine geomorphology of the area, between the Betsiamites River and Rimouski (Figure 1), is characterized by yet larger landslide scars and accumulation of debris. A 54 km^2 landslide scar, characterized by two topographic depressions on the submarine shelf separated by a 5 km^2 central butte of intact deposits, and a 104 km^2 related debris lobe in the Laurentian Channel, makes up the most significant landslide scar identified in the St. Lawrence estuary (Cauchon-Voyer et al., 2008). This event, hereafter named the Betsiamites landslide event to differentiate it from the 1663 Colombier landslide event, was relatively dated at 7250 calibrated years (cal) BP (Cauchon-Voyer et al., 2008) by mapping seismic reflections from the top of the debris accumulation in the Laurentian Channel to the location of core MD99-2220 where a chronostratigraphy is available (St-Onge et al., 2003). Similar chronostratigraphic correlations were used to date another layer of buried debris flow deposits as older than 9250 cal BP. This layer is found below the 7250 cal BP Betsiamites submarine landslide scar on the shelf (Cauchon-Voyer et al., 2008). This correlation method introduces a possible error of a few hundred years, but regardless of these uncertainties, it provides enough evidence to attribute the large submarine landslide scars and debris deposits to the results of events well before the recent Colombier landslide. Elsewhere in the Estuary, other authors have identified and described submarine landslide scars (e.g., Massé and Long, 2001; Duchesne et al., 2003; Lajeunesse et al., 2007; Campbell et al., 2008; Gagné, 2008; Locat et al., 2008; Mosher, 2008), but no other landslide scars of dimensions similar to the 7250 cal BP event have been observed on the seafloor.

Any in-depth analysis of large mass movements requires knowledge of the geomorphology, geometry, lithostratigraphy, and geotechnical characteristics of the sediments involved in the failures. For the Betsiamites landslide complex, studies onshore provided only a general description of the geomorphology and age estimation for the landslide event (Bernatchez, 2003). Submarine morpho-sedimentological analysis led to the identification and dating of scars and subaerial debris deposited underwater (Cauchon-Voyer et al., 2008). These studies did not define the material involved nor the physical link and sequence between the subaerial and submarine events. Understanding the mechanisms involved in the failure of such large mass movements, which left related scars and debris above and below the shoreline, is necessary for coastal landslide hazard assessment. For example, Highway 138, which is the main road and lifeline on the North Shore of the St. Lawrence estuary, runs directly across the Colombier landslide scar and is constructed on many other similar deltaic complexes along the North Shore. This fact underscores the need for assessment of the probability of occurrence of similar events.

The objectives of this paper are to understand the events that produced the large Betsiamites landslide complex in order to assess the potential of coastal geohazards such as landslide in the St. Lawrence estuary. In this paper, the subaerial and submarine geomorphology of the Betsiamites landslide complex and its surroundings is presented first. The seismostratigraphic sequence obtained along the shoreline is then presented and correlated with lithostratigraphic and piezocone test data. These data are then integrated in order to interpret the morpho-stratigraphy prior to failure and define the landslide events and sequences that occurred in the area. The links between the subaerial and submarine scars are demonstrated. This paper comes as a first step for subsequent slope stability and post failure flow dynamics analyses (Cauchon-Voyer, 2011).

2. Physical setting

2.1. Local physiography

The Betsiamites River flows eastward into the St. Lawrence estuary (Figure 1a) and truncates a large coastal plain that is about 7.5 km wide by 25 km long and interrupted by several marine terraces, bedrock outcrops, peat bogs, and raised beach ridges (Bernatchez,

2003). The highest, but intermittent, raised marine terrace in the vicinity of the Colombier subaerial landslide scar is located at about 70 m, whereas bedrock outcrops reach elevations up to 140 m. Underwater, the regional morphology of the Estuary is divided into three physiographic regions: the shelf (SH) bounded by a shelf break (SB) lowering to the Laurentian Channel (LC) (Figure 1b). The shelf has an average width of 10 km and a maximum slope of 2°, with water depths ranging from the shoreline to about 150 m. The shelf break occurs between 150 and 200 m water depth, creating a slope of about 10° with maximum height of 200 m. The Laurentian Channel is a long sub-horizontal topographic depression in the seafloor of the Estuary with maximum water depth of 375 m and width of 45 km in the study area. The study area is located between the Lower St. Lawrence Seismic Zone (LSZ) and the Charlevoix Seismic Zone (CSZ) (e.g., Adams and Atkinson, 2003), implying that the area frequently undergoes earthquakes. Since these seismic zones started being monitored in the late 19th century several earthquakes with magnitude ranging between 4.5 and 6.5 were recorded (e.g., Lamontagne et al., 2003; Lamontagne et al., 2008).

2.2. Late Quaternary history

The study area was covered by the Laurentide Ice Sheet during the late Wisconsinan. Following deglaciation, which started around 12 kyr BP in the area, the combined effect of the glacio-isostatic subsidence and eustatic sea-level rise resulted in the marine invasion of the Goldthwait Sea up to an elevation of 152 m above present sea-level around 11 kyr BP (Bernatchez, 2003). Subsequent land emergence led to the erosion of deltaic plains resulting in the stair-like morphology of raised marine terraces visible onshore. At the time of the large submarine failure, dated at 7250 cal BP, relative sea level had reached more or less its present level (Dionne, 2001; Bernatchez, 2003).

It is generally accepted that the lithostratigraphic Quaternary sequence found on the subaerial portion of the delta and area is limited to deposits of the last glaciation and deglaciation (e.g., Dredge, 1976; Dubois, 1977; Dionne and Occhietti, 1996; Bernatchez, 2003). The coastal subaerial stratigraphy of the Betsiamites River area is simplified, from bottom to top, as a sequence of marine, prodeltaic, fluvio-deltaic, intertidal, and littoral deposits.

Offshore, many authors described the seismostratigraphy in the St. Lawrence estuary (e.g., Syvitski and Praeg, 1989; Josenhans and Lehman, 1999; Massé, 2001; Duchesne et al., 2007; Duchesne et al., 2010). Such analyses provide an interpretation of the Quaternary stratigraphy based mostly on geophysical interpretation with limited geological validation (e.g., long boreholes). Syvitski and Praeg (1989) defined 5 seismic units and proposed a geological interpretation associated with the retreat of the Laurentide Ice Sheet in the Estuary, which is still used today. From the base to the top, these seismic units are interpreted as: (U1) ice-contact deposits including ice-loaded and ice-deposited sediments such as tills; (U2) ice proximal, coarser grained sediments deposited as a thin conformable layer during rapid retreat of an ice terminus; (U3) fine-grained ice-distal sediments probably correlated to the Goldthwait Sea clays (e.g., Dionne, 1977); (U4) coarser paraglacial sediments transported from land to sea from a rapidly ablating subaerial ice-sheet; and (U5) postglacial sediments deposited under modern sea-level and oceanographic conditions. Cauchon-Voyer et al. (2008) identified the same seismostratigraphic sequence for the submarine portion of the Betsiamites River delta area. Despite these numerous geophysical studies, very few provide geological validation with core data. St-Onge et al. (2003) studied and described a 51.6 m-long piston core located in the Estuary; MD99-2220 shown in Fig. 1, and dated the deposition of two lithological units. They were interpreted as glaciomarine and postglacial sediments and subsequently correlated to seismic units U3 and U5 (Cauchon-Voyer et al., 2008; Barletta et al., 2010). Seismic unit U2 was sampled on the southern shelf of the Laurentian Channel and is also interpreted as ice-proximal glaciomarine sediments (St-Onge et al., 2008).

3. Data and methods

Onshore, the approach used to interpret the geometry of the area prior to the landslide events and the location of the failure surfaces included integration of piezocone soundings (CPTU), subaerial seismic reflection data, and boreholes. Offshore, integration of geophysical and sampling results allows the linkage of the submarine landslide morphostratigraphy to the subaerial observations (Syvitski and Praeg, 1989; St-Onge et al., 2003; Cauchon-Voyer et al., 2008). It is important to notice that such integration of both onshore and offshore investigations is very seldom done and implies the use of many different techniques.

3.1. Digital terrain models

The description of the landslide complex includes a morphological analysis, aerial photo interpretation, and geometrical measurements carried out on the subaerial and submarine digital elevation models (DEM). The subaerial DEM was derived at a 1 m resolution from airborne laser scanning (LIDAR) and hypsometric lines at 1 m contour interval obtained from photogrammetry on 1:15000 aerial photos. Details on the bathymetric data used to obtain the submarine DEM are found in Cauchon-Voyer et al. (2008). Landslide volume calculations were carried with ArcGIS Spatial and 3D Analyst tools.

3.2. Seismic reflection data

A continuous seismic reflection profile was acquired over a total length of 5.2 km along the shoreline west of the Betsiamites River (see location in Figure 1) and offers a cross-section perpendicular to the north–south axis of progradation of the delta. Sub-bottom profiling allows definition of seismic properties of subsurface materials from reflected seismic waves, from which geological interpretation such as sediment type and accumulation pattern are proposed. Seismic reflection data were acquired using an array of 24 geophones (40 Hz) at 5 m spacing. The source was a “Buffalo gun” firing 12-gauge blank charges that were in holes about 50 cm below the ground surface (Pullan and MacAulay, 1987). The configuration for the survey was a repetition of 12 shots increasing at 5 m steps, the first shot being fired at 2.5 m away from the first geophone. The data were acquired with a Geometrics Strata Visor seismograph and processed with the WinSeis Turbo software. Normal moveout corrections were applied to account for changes in distance between the source and each receiver. Stacking velocities were determined during the processing and a constant speed of 1500 m/s was used to linearly convert two-way travel time to approximate depths. Band pass filtering (150–200 and 500–600 Hz) was also applied to the presented section. In addition, 750 km of high-resolution seismic reflection data (white lines in Figure 1) used in this study were obtained with an EG&G chirp system (2 to 12 kHz) mounted on board the Coriolis II research vessel (Cauchon-Voyer, 2007). To simplify, sections and descriptions presented in this paper are directly converted to depths. Interpretation of subsurface data was performed with the Kingdom Suite software package. Distinct seismic facies were defined according to amplitude and geometry of the inner reflections and to characteristics of the upper transition of each facies. In definition of subaerial seismic facies, the upper 10 ms were considered to be impacted by surface waves and hence do not necessarily reveal the inner geometry of the first 7.5 m of the deposits.

3.3. Piezocone tests (CPTU)

Thirty-eight piezocone tests, i.e., cone penetration tests with pore water pressure measurement (CPTU), were performed on both shores of the Betsiamites River (Figure 1b). These tests provide continuous

in-situ geotechnical measurements of soil resistance and pore water pressure induced by penetration of the cone (e.g., Lunne et al., 1997). They were carried out with a 15-ton capacity cone with a 15 cm^2 base area. To obtain a better definition of the stratigraphy, the penetration rate was maintained at 10 mm/s and pore pressure measured immediately behind the tip (u_{base}) and tip resistance (q_c) were recorded at 10 mm intervals. Tip resistance (q_c) was corrected for the pore pressure acting behind the tip to obtain (q_t). The penetration depth of the CPTUs varies from 3.35 to 59.9 m. Pore pressure dissipation tests were carried out when coarser layers of higher resistance where reached and at the end of all soundings. The distance over which the cone senses an interface increases with material stiffness, indicating that soft layers thinner than 10 cm can be detected whereas stiff layers may need to be as thick as 75 cm or more for the cone resistance to reach its representative value (Lunne et al., 1997). When sounding results are used for geotechnical correlations, tip resistance is presented in terms of net tip resistance ($q_t - \sigma_{vo}$). Variation with penetration of the values of net tip resistance and induced pore water pressure, in addition to the shape (e.g., continuous or highly layered) and the slope of the profiles were considered for correlations between soundings.

3.4. Core data

Two boreholes were performed in the area (Figure 1b). Borehole F46010, to a depth of 58.9 m, was performed in the accumulation zone of the subaerial landslide (68°44′20.1″W–48°53′46.9″N) at a distance of 75 m from the shoreline and at an elevation of 7.8 m above sea-level. Unless specified otherwise, all data are positioned corresponding to their elevation above (positive value) or below sea-level (negative value). Borehole F46006, to a depth of 54.4 m, was performed 400 m behind the escarpment of the Colombier subaerial landslide scar (68°46′6.9″W–48°54′12.0″N) at an elevation of 47.6 m. One Nilcon vane test profile was carried out at site 46006 to estimate the in situ undrained shear strength. Samples were recovered with a split spoon sampler and Shelby sampling tubes (70 mm diameter × 76 cm length). Immediately after recovery, sediments were subsampled at all sample ends in order to measure water content and to assess sample preservation. Digital X-ray images of all samples before extrusion were obtained with computerized co-axial tomography (CAT-Scan). The samples were then cut in subsections of 5 to 15 cm, described, covered with a mixture of petroleum jelly and paraffin, and kept undisturbed in a cold room (~8° and 88% humidity). Natural water contents, shear strength measured with the Swedish fall cone, Atterberg limits, and preconsolidation pressures were subsequently measured. The preconsolidation pressure (σ'_p) was determined by conventional 24 h oedometer tests with load increment of 0.5 using the Casagrande method. Grain size distributions were obtained using a Beckman Coulter LS 13 320 laser diffraction particle size analyzer for the sediment fraction smaller than 2 mm. Sediment mineralogy was identified by X-ray diffraction analyses (XRD) from analyses on bulk samples and sediment fractions smaller than 2 μm. Salinity values were estimated by ion chromatography. Forty-six sediment samples were also recovered in the submarine segment of the delta (Cauchon-Voyer, 2007) and the location of the sampling stations are also indicated in Fig. 1b. Nine marine shell fragments from boreholes F46010 and F46006 were sampled and ^{14}C dated by accelerator mass spectrometry (AMS) at the AMS facility of the University of California, Irvine (Table 1). To account for the apparent age of the dissolved inorganic carbon reservoir, a correction of −400 years was applied ($\Delta R = 0$). To convert the ^{14}C conventional ages to calendar years, the dates were calibrated using the CALIB 5.0.1 online software (Stuiver and Reimer, 1993).

4. Surface geomorphology

The subaerial and submarine portions of the delta are characterized by various geomorphologic elements resulting from landslide events. In this section, the subaerial domain is presented first, followed by the description of the submarine domain, with emphasis on both the local morphology and the elements resulting from mass movement events.

4.1. Subaerial morphology

In the vicinity of the Colombier landslide scar, large outcrops of Late Proterozoic Grenvillian metamorphic rocks (Franconi et al., 1975) break the highest deltaic plains at elevations ranging between 60 and 140 m (Figure 2). One of these outcrops is located at a distance of 200 m north of the landslide scar at an elevation of 60 m. The bedrock outcrops also on the shoreline at sea-level on the west side of the site (Figure 2), implying that the bedrock surface drops for at least 60 m over a distance of about 1500 m.

The subaerial topography around the landslide scar is composed of 4 main levels of raised marine terraces at elevations ranging between 70 and 15 m (Figure 2). The upper 70 m terrace is found in disconnected sections above the landslide scar. The 60 m terrace is completely truncated by the landslide scar. The terrain at 60 m is overlain by peat bogs and has a slope angle of less than 1°. West of the landslide scar, shown on the left side of Fig. 3a, the 40 m terrace runs parallel to the terrace at 60 m and is also truncated by the landslide scar (Figure 3b). The slope of the terrain above the landslide on the 40 m terrace is around 0.5°. East of the scar, many well-defined raised beach ridges are visible on the surface of the 40 and 15 m terraces and their orientations shift as they lower in elevation (Figure 2). The 15 m terrace is seen mainly east of the landslide scar and its upper plain narrows as it approaches the 40 m terrace (Figure 2).

For the Colombier subaerial landslide body, four morphological zones are defined on the basis of their geomorphologic elements and are referred as the West, Central, East, and Accumulation zones (Figure 3a).

Table 1
Radiocarbon dates on shell fragments.

Borehole	Elevation (m)	Conv. age ^{14}C (yr BP)	Conv. age ^{14}C − 400 yr (yr BP)	Calibrated age (cal BP)	Lab#
F46006	19.57	9265 ± 20	8865 ± 20	10136	UCIAMS-66258
F46006	15.55	9625 ± 25	9225 ± 25	10508	UCIAMS-60876
F46006	9.97	9725 ± 25	9325 ± 25	10570	UCIAMS-60872
F46006	9.41	9745 ± 25	9345 ± 25	10585	UCIAMS-60874
F46010	−15.27	9365 ± 20	8965 ± 20	10203	UCIAMS-66260
F46010	−24.17	9350 ± 25	8950 ± 25	10194	UCIAMS-60873
F46010	−32.07	9830 ± 20	9430 ± 20	10666	UCIAMS-66259
F46010	−34.97	9770 ± 25	9370 ± 25	10609	UCIAMS-60875
F46010	−38.05	9850 ± 25	9450 ± 25	10697	UCIAMS-66261

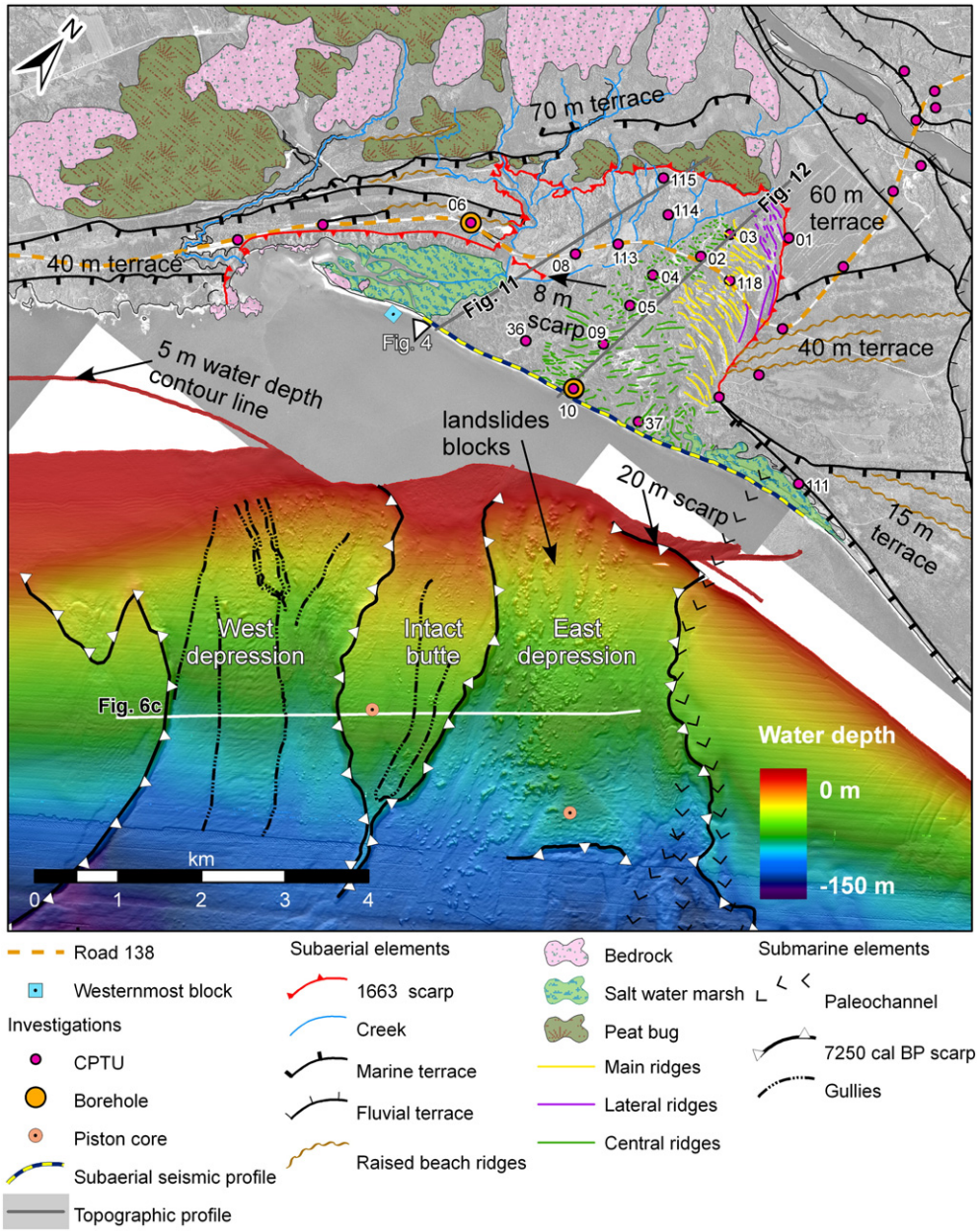

Fig. 2. Geomorphologic interpretation of the Betsiamites landslide complex area.

The West zone consists of a salt water marsh bounded to the north by a 45 to 50 m escarpment with an average slope of 15°. This escarpment runs parallel to the 60 m terrace for 3000 m, then drops to sea level and truncates the 40 m high marine terrace (Figure 3b). This escarpment is subjected to small shallow landslides. Bedrock outcrops are also found at sea-level in this area.

The Central zone is characterized by a regular southeast sloping terrain of average slope of 2.5° bounded to the north by an upper escarpment with a surface elevation decreasing from 60 to 45 m. The height of this escarpment ranges between 10 and 30 m and its slope angle varies between 15° and 25°. This escarpment and the underlying terrain are eroded by small creeks (Figure 2) which drain the northwest terrain above the landslide. In the lower portion of this zone there is an escarpment with a maximum height of 8 m (pointed by an arrow in Figure 3c) at an elevation of about 10 m. This escarpment has more or less the same orientation as the escarpment of the West zone and is truncated to the west by road works and gully erosion (Figure 3c).

The main morphological characteristic of the East zone is a succession of elongated ridges and depressions (Figure 2). This part of the Colombier landslide scar has a morphology typical of a spread such as described by Cruden and Varnes (1996). Three main orientations of ridges are observed. The first group, in the northern part (main ridges, yellow in Figure 2), has an E–W orientation (90°). These ridges have a typical height, width and length of 10 m, 40 m and 200 m, respectively. The second group, to the east (lateral ridges, purple in Figure 2), has an average orientation of 120°. These ridges are slightly larger than the E–W ridges and have an average length of 275 m and maximum heights and widths of 25 and 60 m. The largest ridges are still connected to the eastern flank. The height of the scarp in this area ranges between 25 and 30 m. The third group of ridges has (central ridges, green in Figure 2) an orientation of 230°.

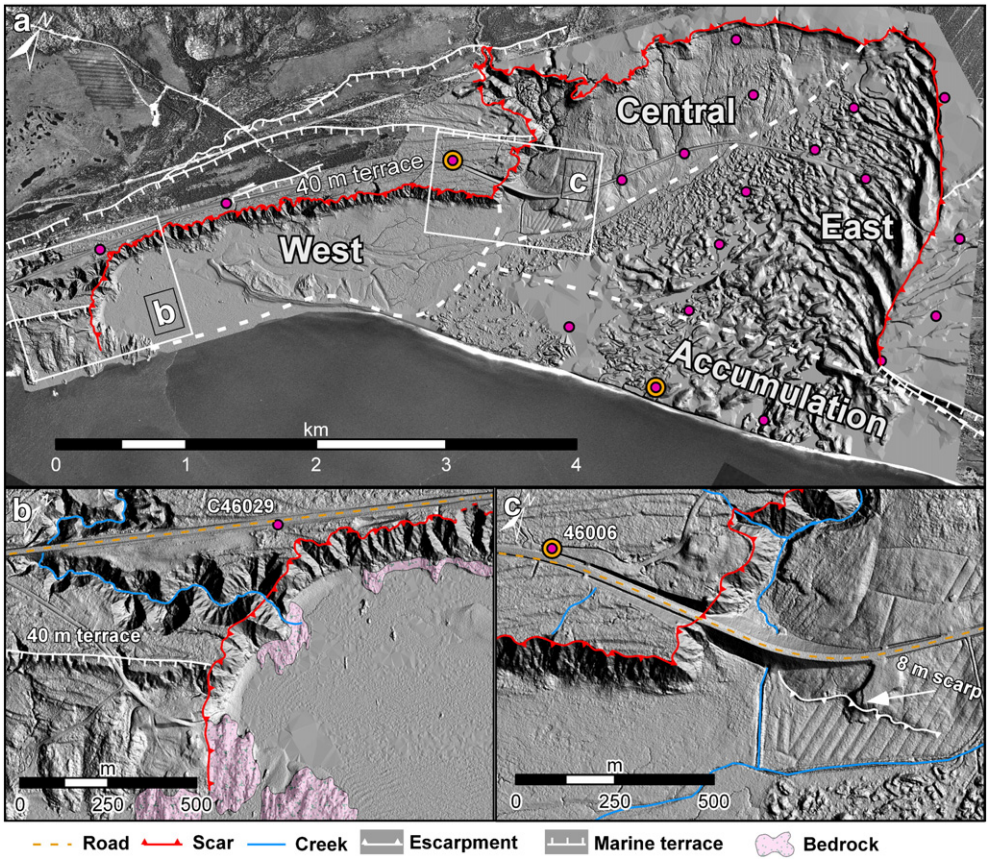

Fig. 3. Digital elevation model of the Colombier subaerial scar. a) Morphological zones with geomorphologic characteristics within the subaerial landslide body and CPTU locations. See text for details; b) enlargement of the western escarpment; c) enlargement of the area with the 8 m scarp within the central zone.

The Accumulation zone of the landslide is defined as the subaerial area where the displaced material deposited. This zone includes a leveled and forested area with an average elevation of 5 m, and the beach near or at modern sea-level. Disorganized ridges are also observed in this zone (central ridges, green in Figure 2). This zone appears to be an extension of the landslide debris in the Estuary. On

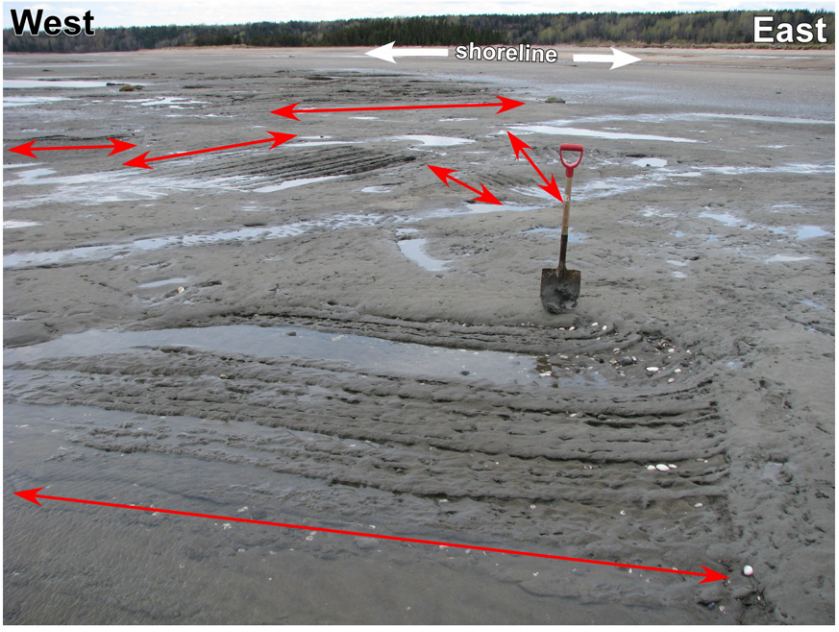

Fig. 4. Beach at low tide revealing blocks of deformed clayey sediments currently eroded by marine action. Arrows are parallel to stratifications (typically 10 cm-thick) in the landslide blocks. Position of image is indicated in Fig. 2 by a white triangle.

the beach at low tide, large blocks of deformed and rotated sediment beds (Figure 4) are observed. These blocks extend into the West zone and the position of westernmost block observed at low tide is marked by a blue square in Fig. 2. As it will be demonstrated later, the northern limit of the Accumulation zone is approximately the interpreted location of the marine terrace prior to the landslide.

4.2. Submarine morphology

The main geomorphologic element on the shelf is a 54 km^2 landslide scar, with two main topographic depressions, the West depression and the East depression, separated by an intact butte with steep flanks and flat top (Figure 2). This submarine scar resulted from the Betsiamites landslide event dated at 7250 cal BP and was partly filled by debris of the 1663 Colombier landslide event (Cauchon-Voyer et al., 2008). It is assumed that the submarine scar resulted from one event dated at 7250 cal BP, but it may have resulted from more than one failure phase. Both depressions have widths ranging from 2 to 4 km, lengths of 7 km, and floor slopes of about 1°. The height of the flanks to the seafloor of both depression ranges from 12 to 20 m. The butte is 5 km^2 in area with a maximum length and width of 4.5 km and 1.6 km respectively (Figure 2). The average slope of the top of this butte is 1°. The depressions and the butte are overlain by 3 to 10 m of subaerial landslide debris. The scar extends from −10 m to −140 m (Figure 5).

The northernmost ship track of the bathymetric survey closest to the shore follows approximately the 5 m water depth contour line (Figure 2). This contour does not run parallel to the shoreline but instead moves seaward as it approaches the West depression. The upper portion of the West depression is smooth, has a fairly low slope of about 0.5°, and no apparent escarpment (Figure 2). The easternmost portion of the East topographic depression has a low gradient and is overlain by landslide blocks. The westernmost portion is bounded by a 20 m high escarpment having a slope of 8° and running parallel to the shoreline (Figure 2). As it will be demonstrated, this escarpment has a significant impact on the stability of the submarine area and is interpreted as the back escarpment of the submarine failure dated at 7250 cal BP. Fewer blocks appear at the toe of this escarpment than in the easternmost portion of the East topographic depression.

Offshore, in the Laurentian Channel (Figure 1), there is a large depositional lobe observed at an average water depth of 350 m covering an area of about 104 km^2 (Figure 5). It has a maximum width of 15 km and an average thickness of 9.4 m, thus has an estimated volume of ~1 km^3. This lobe corresponds to the sediments mobilized from the shelf to the Laurentian Channel by the 7250 cal BP Betsiamites submarine landslide (Cauchon-Voyer et al., 2008). Seismic profiling and samples recovered from the lobe area indicate the presence of a few cm-thick turbidite layer associated with the 1663 Colombier landslide event on top of hemipelagic sediments covering the 7250 cal BP debris (Cauchon-Voyer et al., 2008).

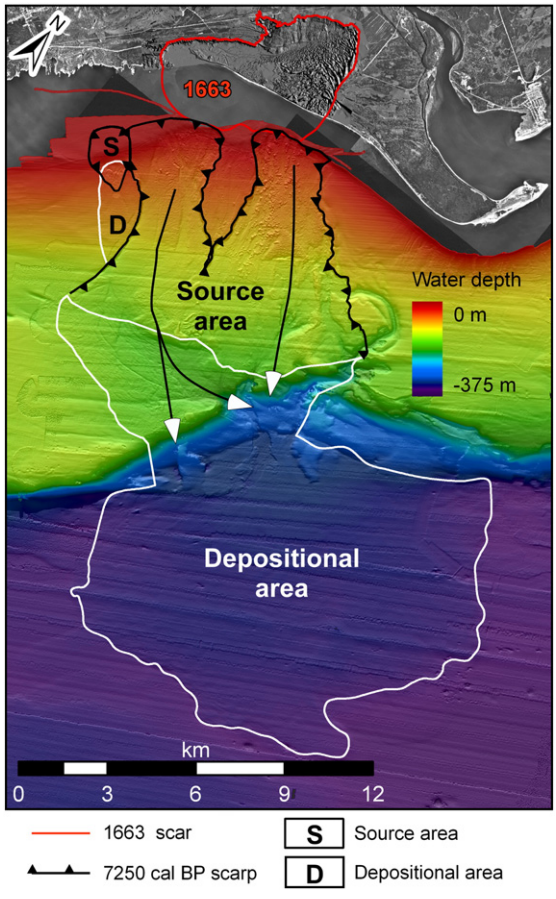

Fig. 5. Source and depositional areas of the 7250 cal BP Betsiamites submarine landslide event.

5. Coastline seismostratigraphy

The 5.2 km-long subaerial seismic reflection profile shown in Fig. 6a provides correlation between the boreholes and CPTUs in addition to linking the subaerial stratigraphy (Figure 6b) to the submarine seismostratigraphy (Figure 6c). Four seismic units and a reflector resulting from a strong acoustic impedance contrast, interpreted as bedrock, were identified on the seismic section (Figure 6b) and are summarized in Table 2. The lower four subaerial units correlate with the seismostratigraphy interpreted offshore for the Betsiamites River area (Figure 6c) (Cauchon-Voyer et al., 2008). For consistency with previously published work, the numbering and interpretation proposed by Syvitski and Praeg (1989) are followed.

The sediment–bedrock interface is characterized by relatively continuous high amplitude reflections, where little energy penetrates below this boundary. The depth to the bedrock decreases west to east, from −120 to −30 m, on the profile. The bedrock drops at an angle of about 4° for the first 1000 m and then reaches a more gently sloping segment with an angle of less than 0.5°. Additionally, the bedrock outcrops on the beach 600 m west of the seismic profile, which supports the interpretation that the continuous high amplitude reflections correspond to the sediment–bedrock interface.

Seismic unit U1 is the lowermost seismostratigraphic unit characterized by moderate to strong amplitude reflections and poor or absent continuous internal reflecting horizons. The upper bounding surface is highly variable. The thickness of unit 1 ranges from 1 to 43 m and averages 29 m. This unit was associated to ice-contact deposits including ice-loaded and ice-deposited sediments (Syvitski and Praeg, 1989).

Seismic unit U2 is characterized by highly variable acoustic reflections with strong and closely spaced reflecting horizons. The upper boundary of this seismic unit corresponds to a sharp decrease in amplitude of the reflecting horizons. The thickness of unit 2 ranges from 5 to 36 m and averages 17 m. On the easternmost 1500 m of the section, the thickness of U2 increases and has an average thickness value of 25 m. In this section, between 4500 and 5000 m, the reflecting horizons of the upper boundary have a V-shape dipping down 15 m over a total distance of 500 m, which is interpreted as a buried submarine channel. This unit was defined as ice proximal, coarser grained sediments deposited as a thin conformable layer during the rapid retreat of an ice terminus (Syvitski and Praeg, 1989). As it will be shown, the upper part of this unit has been sampled in borehole 46010.

Seismic unit U3 consists of low amplitude reflections and presents only few weak continuous reflecting horizons located in the lower portion of the seismic unit. The upper transition of this unit with U4 is

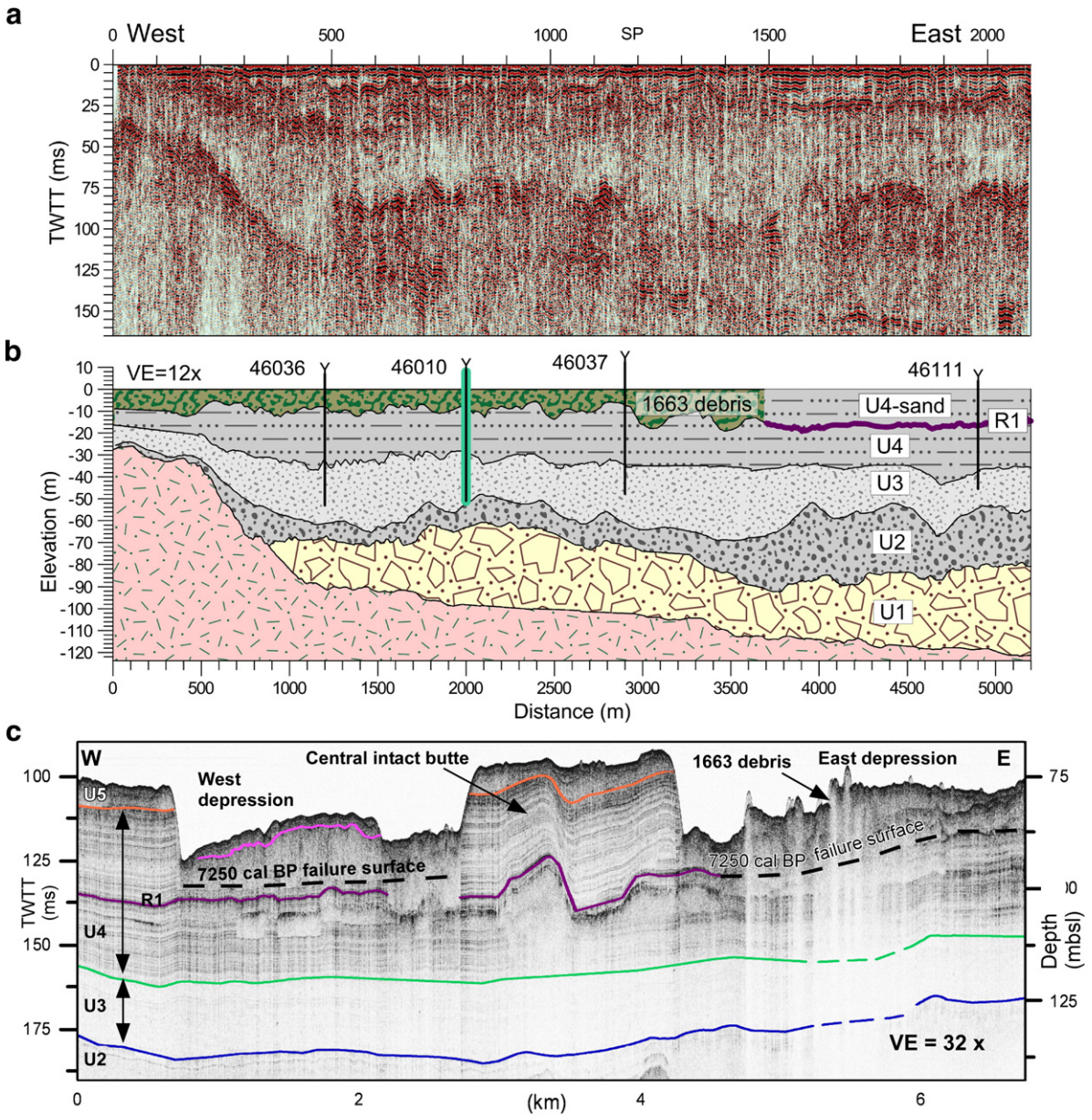

Fig. 6. Seismostratigraphy of the Betsiamites landslide complex. a) 5.2 km-long continuous subaerial seismic reflection profile; b) seismic interpretation. The vertical black lines indicate the locations and depths reached by the four CPTUs carried out close to the shoreline whereas the green line indicates the location and depth reached in borehole 46010. VE = 14×; c) Submarine seismostratigraphy, modified from Cauchon-Voyer et al. (2008). 9250 corresponds to the seismic body interpreted as debris of a submarine landslide dated as older than 9250 cal BP (see text for details). TWTT = two way travel time. The depth scale was approximated using a constant velocity of 1500 m/s. Position of submarine profile is indicated in Fig. 2, view looking north toward the head of the landslide.

weak and often absent, i.e., the change in acoustic impedance is too weak to obtain coherent reflections. The boundary was interpreted mostly on the general trend of reflection amplitude, i.e., U3 being generally weaker than U4. The transition between both units is hence approximate. The thickness of U3 ranges between 7 and 34 m with an average of 22 m. This unit was interpreted as fine-grained ice-distal sediments (Syvitski and Praeg, 1989) probably correlated to the Goldthwait Sea clays (e.g., Dionne, 1977; Dredge, 1983).

Seismic unit U4 is a stronger amplitude section with strong and coherent internal reflections. The thickness of U4 ranges between 8 and

Table 2
Summary of seismic units on the subaerial profile.

Subaerial seismic units	Geological interpretations	Reflecting horizons pattern	Thickness (m) min (average) max
U1	Ice-contact deposits	Poor or absent continuous internal reflecting horizons	1 (29) 43
U2	Ice proximal, coarser grained sediments	Strong amplitude and closely spaced reflecting horizons	5 (17) 36
U3	Fine-grained ice-distal glacio-marine sediments	Weak continuous reflecting horizons	7 (22) 34
U4	Paraglacial prodeltaic sediments	Closely packed reflecting horizons	8 (25) 44
Upper facies	Landslide debris	Reflecting horizons are conformable on unit 4	5 (10) 19

44 m and averages 25. Within this seismic unit, there is a 2 to 4 m thick sequence of closely packed reflecting horizons, which is labeled R1 in Fig. 6b. These reflecting horizons are due to strong acoustic impedance contrasts in the sedimentary succession that could result, among other causes, from a significant change in grain size distribution, e.g., clayey to sandy material. The maximum amplitude of this package of reflecting horizons is recorded at about −16.5 m. Similar reflecting horizons within Unit 4 were mapped on the submarine profiles on the submarine shelf (Figure 6c) (Cauchon-Voyer et al., 2008). This unit correlates to paraglacial sediments transported from land to sea from a rapidly ablating subaerial ice-sheet (Syvitski and Praeg, 1989).

The uppermost seismic facies is apparent in Fig. 6c in the westernmost part of the profile. Reflections are conformable on the irregular and hummocky unit 4. This facies is not numbered as it does not correspond to the post-glacial sediments defined by Syvitski and Praeg (1989) as unit 5. The average thickness of this seismic facies is 10 m. The seismic amplitude of this facies varies and based on seismic characteristics from the literature (e.g., Piper et al., 1999) is interpreted as subaerial landslide debris.

6. Lithological units

Two subaerial boreholes provide lithological data to validate seismic reflection interpretations. Sedimentological and geotechnical data obtained from borehole 46010 (Figure 7) and borehole 46006 (Figure 8) are summarized in Table 3 whereas the lithostratigraphic correlations are presented in Fig. 9.

6.1. Borehole in subaerial slide debris—site 46010

Lithological and geotechnical data for the landslide debris and the deposits below the failure surface were obtained from the 58.9 m long borehole F46010 (Figure 7) carried out 40 m from CPTU C46010 (see location in Figure 2) at an elevation of 7.8 m along the shoreline. Six lithological units, with different sedimentological and geotechnical properties, were identified (Table 3).

The lowermost lithological unit (10-L2) consists of gravelly and bouldery sandy silt. On the CPTU profile, this lithological unit is characterized by more than 4 m of closely spaced layers of moderate (3 MPa to 18 MPa) net tip resistance ($q_t - \sigma_{vo}$). Pore pressure dissipation tests carried out within this unit indicated hydrostatic conditions with reference to the water table at an elevation of 4.7 m. This unit corresponds to the upper portion of seismic unit U2 (Figures 6b and 9).

The second lithological unit (10-L3a) consists of gray laminated silt to silty sand with some clay with generally low net tip resistance. This unit is about 4 m thick and shows a decrease in net tip resistance with increasing depth. It correlates with the lower portion of seismic unit U3 (Figures 6b and 9).

The third unit (10-L3b) observed in this borehole comprises bioturbated gray silty clay. This unit is 21 m thick at elevations between −43 and −22 m. The natural water content ranges between 30 and 43%. The plasticity index ranges between 16 and 28% and the liquidity index is lower than 1, with values between 0.7 and 0.9. The clay fraction (particles less than 2 μm) ranges between 29 and 50%

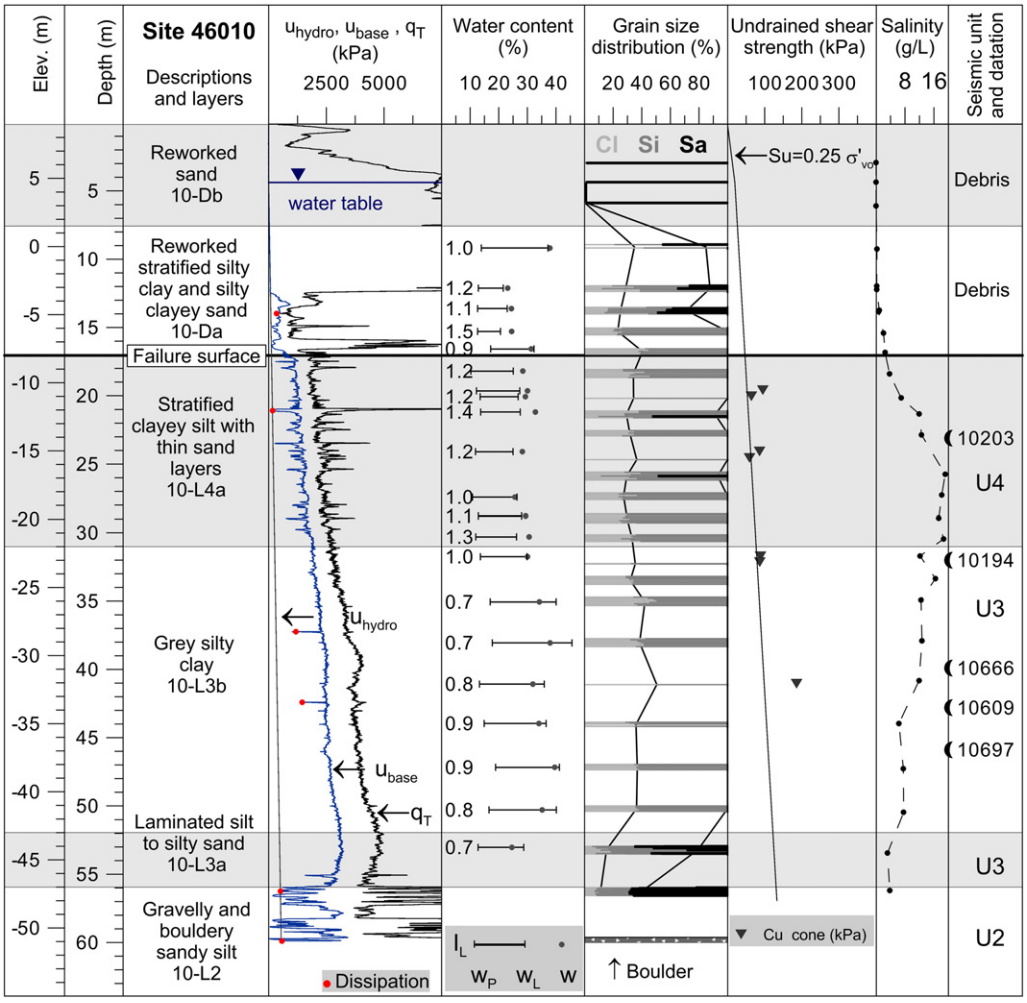

Fig. 7. Geotechnical profile at site 46010 in the accumulation zone of the lateral spread (Phase 3S) of the 1663 Colombier subaerial landslide.

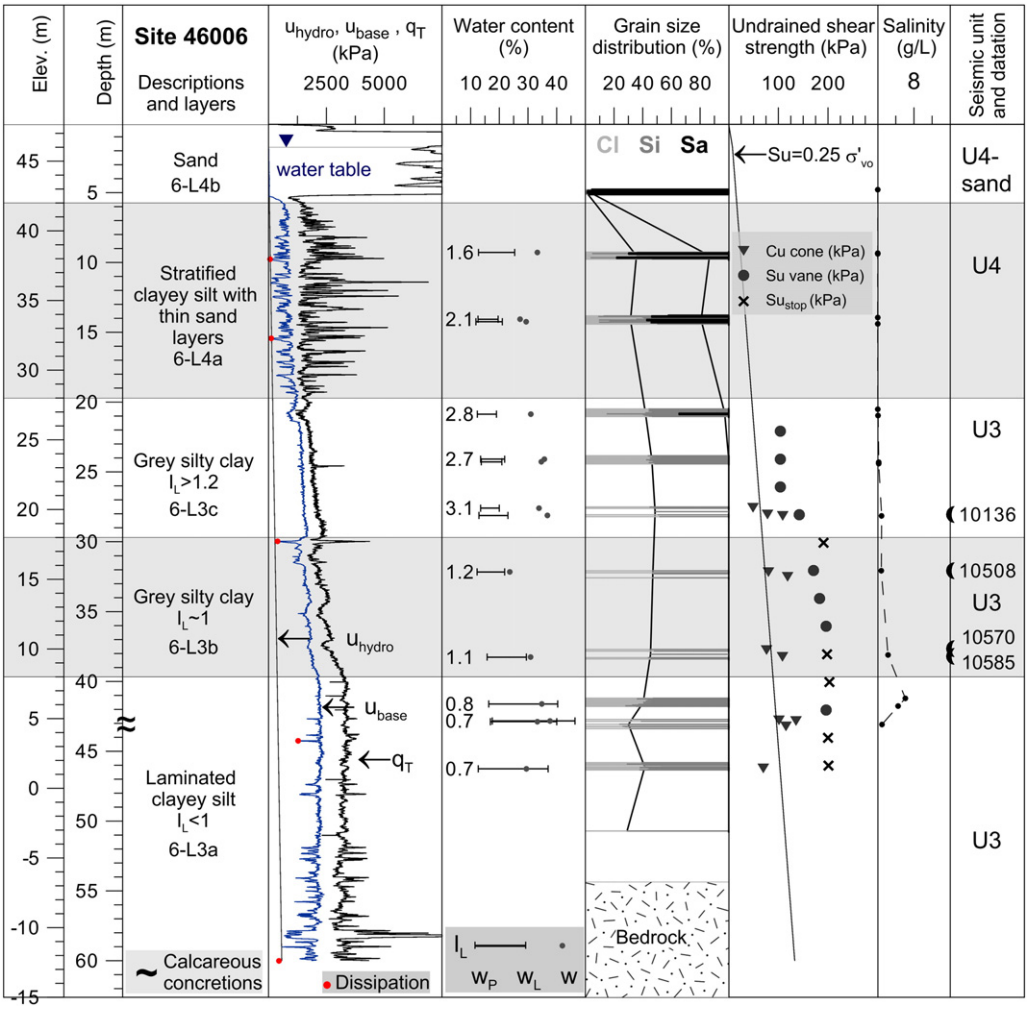

Fig. 8. Geotechnical profile at site 46006 on the upper escarpment of the 1663 Colombier flowslides (Phases 2F and 3F). Cone = Swedish fall cone. Su = undrained shear strength measured with the vane. Su_{min} indicates that the test was stopped at the maximum value of 200 kPa.

and averages 37%. The sensitivity (S_t) values obtained with the Swedish fall cone for this layer are 14 and 56. Salinity values decrease with depth, from 16.4 to 6.3 g/L. Four marine shell fragments sampled within this lithological unit were dated and range between 10.2 and 10.7 ka cal BP (Table 1). This unit correlates also with seismic unit U3 (Figures 6b and 9).

Table 3
Summary of lithostratigraphy and geotechnical properties defined on site, with boreholes and seismic correlations. z = thickness of layer.

Seismic unit	Geological interpretation	Borehole layer	Layer in Figs. 7 and 8	Elevation (m)	z (m)	wn (%)	Ip	IL	St	CF (%)
U2	Coarse ice-proximal glaciomarine sediments	46010 10-L2	Gravelly and bouldery sandy silt	−50.6 6-L to −47	>3.6	–	–	–	–	11
U3	Finer ice-proximal glaciomarine sediments	46010 10-L3a	Laminated silt to silty sand	−47 to −43	4	25	16	0.7	–	15
	Laminated ice-distal glaciomarine sediments	46006 6-L3a	Laminated clayey silt IL<1	8 to ~−12	~20	34	27	0.7	(7–12)	38
	Fine ice-distal glaciomarine sediments	46006 10-L3b	Homogenous gray silty clay	−22 to −43	21	35	22	0.8	(14–56)	37
		46006 6-L3c	Homogenous gray silty clay IL~1	18 to 8	10	27	12	1.1	(35–67)	46
		46006 6-L3c	Homogenous gray silty clay IL>1.2	28 to 18	10	34	8	2.8	(406–1202)	45
U4	Paraglacial prodeltaic sediments	46010 10-L4a	Stratified silty clay and silty clayey sand	−8 to −22	14	29	14	1.2	(13–36)	31
		46006 6-L4a	Highly stratified clayey silt and silty sand	42 to 28	14	30	10	1.9	–	33
U4-sand	Littoral sand	46006 6-L4b	Sand	47.6 to 42	5.6	–	–	–	–	1
Debris	Subaerial landslide debris, i.e., reworked U4- U3	46010 10-D	Reworked stratified silty clay and silty clayey sand	−8 to 1.5	9.5	28	13	1.2	–	30
Debris	Subaerial landslide debris, i.e., reworked U4- sand	46010 10-Db	Reworked sand	1.5 to 9	7.5	–	–	–	–	0.3

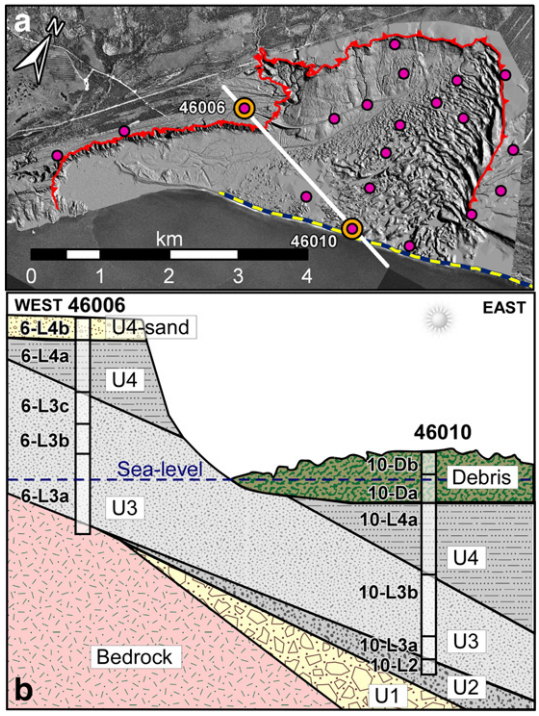

Fig. 9. Schematic summary of the lithostratigraphy and seismostratigraphic interpretation between boreholes 46006 and 46010. Labels in square correspond to seismic units whereas other labels refer to lithological units. Not to scale.

The fourth lithological unit (10-L4a) consists of 14 m of highly stratified silty clay and silty clayey sand between −22 and −8 m. The CPTU pore pressure dissipation test performed in the coarser soil layers of higher resistance indicated hydrostatic conditions relative to the water table. One broken shell fragment was dated in this unit and yielded an age of 10.2 ka cal BP. This lithological unit correlates with seismic unit U4 (Figure 6b) and corresponds to paraglacial prodeltaic sediments deposited in a time of falling relative sea-level (Syvitski and Praeg, 1989; Bernatchez, 2003). This interpretation explains why a date as old as the ones from the previous distal glaciomarine sediments unit (U3, 10-L3b) was sampled within this unit (U4, 10-L4a) since these finer paraglacial sediments are lifted distal glaciomarine sediments eroded and transported from land to sea, which possibly included this remobilized shell fragment.

The fifth lithological unit (10-Da) consists of chaotic facies of silty clay to sandy clayey silt. Evidence of sediment disturbance was observed in five samples, between −8.0 and 0.2 m. The boundary between this chaotic facies (10-Da) and the lower intact stratified silty clay and silty clayey sand (10-L4a) corresponds also to a change in the CPTU profile at −8 m (Figure 7). Three samples between −0.2 and 5.0 m show deformed silty clay clasts in a sandy clayey silt matrix, which is typical of a debris flow deposit (e.g., Mulder and Alexander, 2001). A sample between −6.6 and −5.9 m presents distinctive subvertical 1 cm-thick laminations, implying that this sample was recovered from a displaced block, which had rotated about 90° and that this block was stiff enough to keep laminations intact. The sample recovered at an elevation between −8.0 and −7.4 m represents two facies; the upper 25 cm is a silty layer with subvertical structures sharply overlying a 33 cm-thick layer of silty clay clasts within a sandy muddy matrix. This lithological unit corresponds to the seismic facies interpreted as landslide debris deposits on the subaerial seismic profile (Figure 6b).

Finally, the upper 7.5 m of borehole F46010 contains moderately well-sorted brown sand (10-Db). The water table was 4.3 m below the surface at an elevation of 4.7 m at the time of the soundings. This unit corresponds to regressive paraglacial sand (U4-sand) and, as it will also be demonstrated, was mobilized by the subaerial landslide.

6.2. Borehole outside the Colombier subaerial landslide scar—site 46006

Borehole F46006 (Figure 8) was carried out 400 m from the lateral escarpment of the Colombier subaerial landslide scar close to the West and Central zones (Figure 3). The borehole was located 23 m from CPTU C46006. The CTPU sounding was stopped at 59.99 m, at an elevation of −12.37 m, whereas the borehole reached the bedrock at −6.7 m. This difference implies that the topography of the bedrock is irregular and could drop at a possible angle of 14° between the location of the CPTU and the borehole at site 46006. Four lithological units were defined in this borehole and their characteristics are summarized in Table 3.

The lowermost lithological unit (6-L3a) of borehole F46006 comprises ~20 m of highly laminated clayey silt up to an elevation of 8 m. The clay content ranges between 24 and 53% and this variation results mostly from changes in grain sizes between cm-scale horizontal laminations. Four calcareous concretions were sampled between 4.95 and 4.25 m. They present carbon and oxygen isotope compositions ranging between $-16.8 > \delta^{13}C > -18.4‰$ and $0.43 > \delta^{18}O > 3.4‰$, vs V-PDB, implying that they are typical of glaciomarine concretions (Hillaire-Marcel and Causse, 1989). This unit correlates to seismic unit U3.

The overlying layer (6-L3b and 6-L3c) consists of 20 m of bioturbated gray silty clay between 8 and 28 m. Despite comparable physical characteristics such as grain size distribution and sedimentary structures across depth; it has two layers with different geotechnical behavior and thus is described as two subunits, 6-L3b and 6-L3c. Within both subunits, four marine shell fragments were sampled and dated between 10.1 and 10.6 ka cal BP (Table 1). This unit correlates with seismic unit U3.

Subunit 6-L3b ranges between 8 and 18 m. The natural water contents range between and 24 and 31%. The plasticity index ranges from 10 to 14%, the liquidity index is slightly greater than 1.0, with values ranging between 1.1 and 1.2. The clay fraction is typically of 46%. Sensitivity ranges between 35 and 67.

The upper 10-m thick subunit 6-L3c between 18 and 28 m has a natural water content ranging between 31 and 37%. The plasticity index ranges between 7 and 10% and the liquidity index is greater than 1, with values between 2.4 and 3.1. If a 1-cm thick sand bed at 26.8 m is ignored, the clay fraction ranges between 40 and 52% and averages 46%. The sensitivity values obtained with the Swedish cone, range between 406 and 1202.

According to the radiocarbon dates obtained, the physical characteristics, and the stratigraphic position in the sedimentary column of both subunits of bioturbated gray silty clay, 6-L3b and 6-L3c correlates to the unit (10-L3b) of bioturbated gray silty clay (Figure 9) observed in borehole 46010 (Figure 7). Despite similar sedimentological characteristics, the sensitivity of the material of this layer in 46006 is one order of magnitude greater than that of this layer at site 46010 (Table 2). The fourth lithological unit (6-L4a) within borehole 46006 consists of 14 m of highly stratified clayey silt and silty sand. The natural water contents range between 24 and 40% and the liquidity index is greater than 1.0 with values ranging between 1.6 and 2.8. Some measured remolded shear strength (C_{ur}) values are lower than 0.08 kPa, which corresponds to the limit of the Swedish cone apparatus, indicating that the liquidity index is at least equal or higher than 3.9 according to Leroueil et al. (1983). This lithological unit correlates with seismic unit U4.

The upper lithological unit (6-L4b) is a 5.0 m-thick sandy layer with a sand content ranging from 79 to 97%. Some subsamples within this layer contain 15 to 19% of rounded pebbles of size between 2 and 8 mm. The transition unit 06-L4b with the underlying stratified clayey silt and silty sand (6-L4a) likely corresponds to an erosive contact

related to the lowering of the relative sea-level (e.g., Hart and Long, 1996; Bernatchez, 2003). This unit could correspond to seismic unit U4 according to the interpretation of Syvitski and Praeg (1989) and is labeled U4-sand in this study.

7. Assessment of failure surfaces and material involved in the 1663 Colombier landslide event

Onshore, the boreholes and adjacent CPTUs, provide lithological and geotechnical data inside and outside the Colombier subaerial landslide scar. The subaerial landslide boundaries were obtained from the morphological analysis whereas the seismic profiles allowed the definition of the sequence of deposits and their lateral extension. Combined together, such information allows identification of the materials involved in the 1663 Colombier landslide and detecting the location of the failure surfaces.

7.1. Coastal correlations and failure surfaces

Four CPTUs were carried out along the shoreline (Figure 10) and correlated with borehole 46010. On the subaerial seismic profile (Figure 6a), the upper seismic facies interpreted as reworked sediments reached an elevation of −8.6 m at the location of borehole 46010 (Figure 6b), which is further confirmed by landslide debris identified in the sediment cores (Figure 7). Such lithological interpretation was correlated to the surrounding CPTUs to evaluate the location of a failure surface along the shoreline (Figure 10). The criterion to identify the failure surface on the CPTUs carried out along the current shoreline is the strong change in net tip resistance corresponding to the transition from the chaotic facies (lithological unit 10-Db) to the intact stratified silty clay and silty clayey sand (seismic unit U4 and 10-L4). On that cross section, the failure surface slightly dips toward the center of the delta with a maximum angle of 0.2° (Figure 10). Transitions between the lithological units, interpreted on the CPTUs, also dip toward the center of the delta implying that the failure surface could follow a stratigraphic level resulting from the conformable bedding pattern of the deltaic progradation in the valley. At the location of CPTU C46111 on the eastern side of the site (Figure 2), morphological observations indicate that this site was not impacted by mass movement as it is 1300 m outside the subaerial and submarine scars. The upper 5 m layer within CPTU 46111 is interpreted as regressive littoral sand (U4-sand). At an elevation of −17 m, there is a 35 cm-thick layer with net tip resistance reaching 28 MPa, which, according to Robertson's (1990) charts, is likely composed of a mixture of clean sand to silty sand. The elevation to this sandy layer corresponds to the elevation of seismic reflector R1 identified at about −16.5 m in the subaerial seismic profile (Figure 6b) and correlates to the seismic reflector R1 identified on the submarine seismic profiles (Figure 6c).

7.2. North south correlations and failure surfaces

A sequence of 4 CPTUs (Figure 11) was carried out along the north–south axis of the subaerial landslide in the Central zone (Figure 2). The section in Fig. 11 shows the topography prior to the landslide, estimated according to the location of the remaining terraces and raised beaches, the actual topography, and the location of the failure surface. The final topographic profile discloses an 8 m-high, 500 m long escarpment at 2500 m from the start of the profile (Figure 2). Along this section, from base to top, the four CPTUs present a 1 to 4 m-thick layer presenting the same attributes as coarse ice-proximal glaciomarine sediments (10-L2) identified at site 46010 (Figure 7). This layer is overlain by an uniform layer, likely composed of finer glaciomarine sediments similar to 10-L3a and 10-L3b (Figure 7). The elevation of the failure surface is evaluated on the CPTUs and is defined as the increase of net tip resistance in the profile (Figure 11c). In addition, no other significant irregularity in the profile is interpreted below this level. The failure surface is thus located just below a 3–4 m thick layer of debris. This fact implies that the landslide mass was more than 50 m thick in part of the Central zone but the failed material evacuated the area, which is typical of flowslides in sensitive clay.

A sequence of 6 CPTUs (Figure 12) was carried out in the East zone of the subaerial landslide (Figure 2). The initial topography is assumed according to the topography of the terrain outside the Colombier

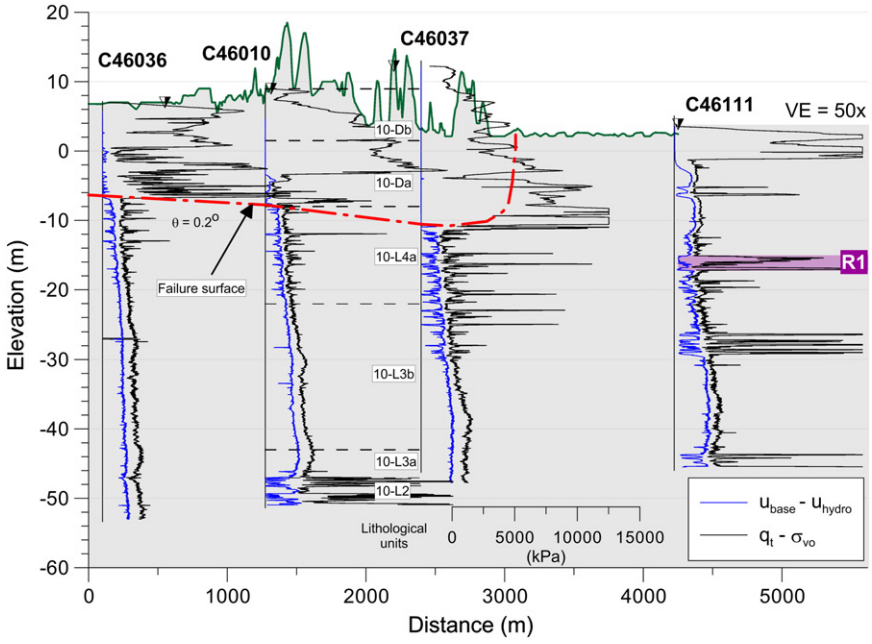

Fig. 10. CPTUs and topographic section along the shoreline. Refer to the triangular symbols for exact CPTU profile locations and to Fig. 2 for topographic profile location.

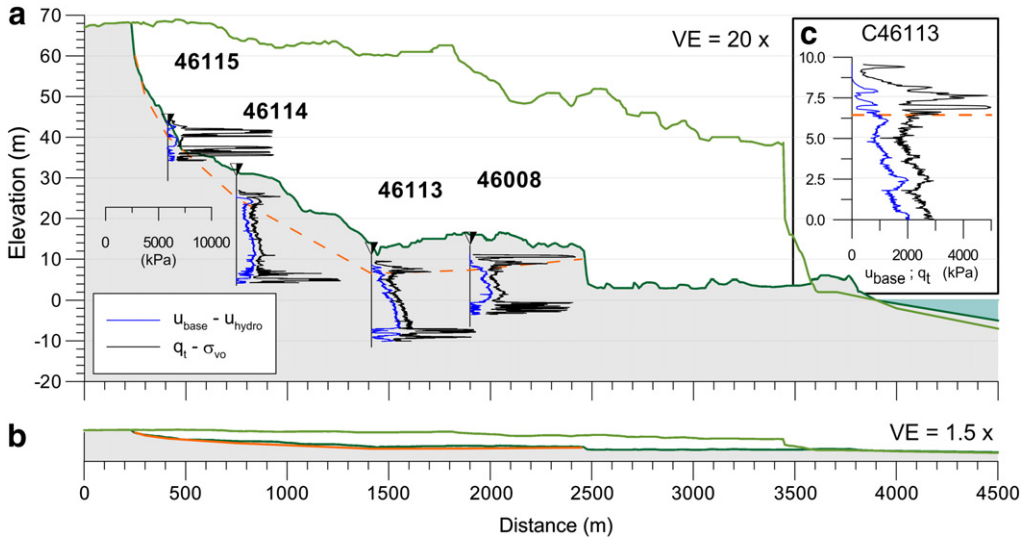

Fig. 11. Sequence of 4 CPTUs carried out in the north south axis of the Colombier subaerial scar in the Central zone. a) CPTUs and topographic profile across the Central area (flowslide 3F); b) profile of the estimated topography prior to failure, failure surface in orange, and final topography at 1.5× vertical exaggeration; c) criterion to define the failure surface in the CPTUs of the central area.

landslide scar. The elevation of the failure surface was evaluated on the CPTU profiles in the East zone when at least one of the three following criteria was met: (1) the profile reveals an apparent decrease in tip resistance (e.g., Figure 13a) as if the mass sliding above the failure surface was remolded; (2) there is a sharp increase in tip resistance (e.g., Figure 13b), as it was seen for the coastal profiles (Figure 10), which could imply that the landslide eroded clayey material and left sandy material above the failure surface; or (3) there is a change in the preconsolidation pressure profile. With an empirical relationship (Eq. (1)) linking preconsolidation pressure (σ'_p) and net tip resistance ($q_t - \sigma_{vo}$) it is possible to emphasize the change in trend of the stratigraphic profiles. These changes can result from marine erosion, landslides or change in soil nature and composition (e.g., Locat et al., 2003).

$$\sigma'_p = \frac{q_t - \sigma_{vo}}{3.4} \quad (1)$$

(Demers and Leroueil, 2002).

For CPTU C46009 (Figure 13c), a 90 cm layer at −17 m is normally consolidated, implying that it could be a layer of remolded and mobilized sediments above the failure surface. Since there is only one borehole (Figure 7) to validate the CPTUs interpretation along the north–south axis (Figure 12), it was not always obvious which

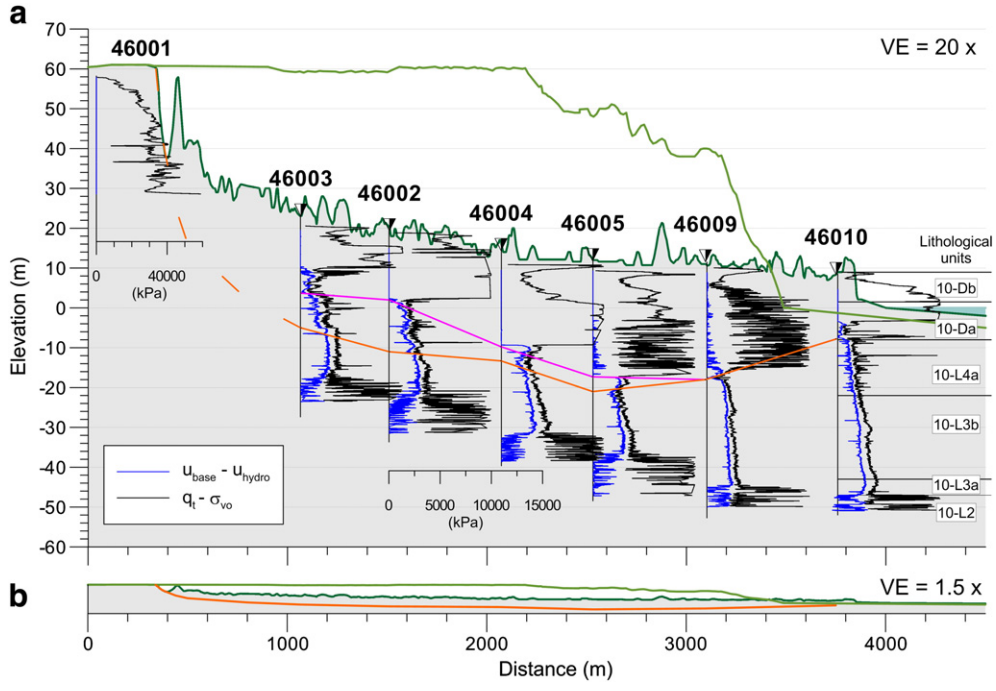

Fig. 12. Sequence of 6 CPTUs carried out in the East zone of the Colombier subaerial scar. a) CPTUs and topographic profile across the East zone of the scar (spread 3S); b) deepest possible failure surface with initial and final topographies at VE = 1.5×.

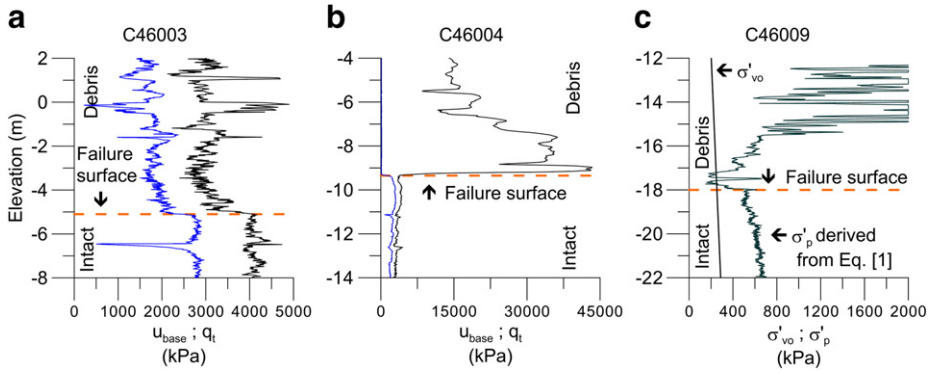

Fig. 13. Criteria used to identify the elevation to the failure surface on the CPTU profiles carried out in the north south axis of the subaerial scar. a) Decrease in tip resistance above a level; b) sharp increase in net tip resistance above a level; c) decrease in calculated preconsolidation pressure.

criterion prevailed and actually corresponds to the failure surface. To account for this ambiguity, two scenarios presenting a shallow and a deeper failure surface are indicated in Fig. 12. The deepest possible failure surface, shown in orange in Fig. 12, developed over a length of about 3 km. The vertical exaggeration of Fig. 12a is 20×, which greatly distorts the perception of the failure surface and emphasizes the fact that it did not need a high gradient to propagate. The slope of the failure surface between C46003 and C46005 is only 0.8°. The slope angle between the interpreted failure surface, which rises up between C46005 and C46010, is 0.45°.

8. Interpretation of seismic data

The subaerial and submarine seismic data show two main features in regard to the landslides that occurred in the Betsiamites area. First, the seismic data allow interpretation of subaerial and submarine depositional processes in the sedimentary succession and of the debris deposits. Secondly, the seismic data allow establishment of the architecture of the deposits along the shoreline and below sea-level and therefore identification of the units of sediments involved in the subaerial and submarine failures.

On the submarine profile shown in Fig. 6c, the transparent seismic package between −110 and −80 m is interpreted as representing mass transport deposits associated with a landslide event dated at 9250 cal BP (Cauchon-Voyer et al., 2008). On the same submarine profile, the truncated reflectors correspond to lateral escarpments of the 7250 cal BP Betsiamites submarine landslide event (Cauchon-Voyer et al., 2008). The 9250 cal BP debris are interpreted within Unit 4 (Figure 6c) below reflector R1, which implies that the 9250 cal BP event occurred before the deposition of R1. The thickest accumulation of 9250 cal BP debris is observed within the central butte of intact deposits within the Betsiamites submarine landslide scar. More than 200 hm^3 of buried deposits over 22 km^2 occurring under seismic reflector R1 (Figure 6c) were mapped across the submarine shelf. The sediment accumulation rate was rapid, up to 34 m/kyr in the Estuary prior to 8500 cal BP (St-Onge et al., 2003), which implies that the depression resulting from the 9250 cal BP event was promptly filled, as seen in Fig. 6c where about 25 m of highly stratified prodeltaic sediments cover reflector R1.

The Betsiamites submarine failure, which removed more than 25 m of deposit within seismic unit U4, occurred above the stratigraphic level of R1 (Figure 6c). In Fig. 6c, the depth to the failure surface is about 20 m below the current seafloor. According to the seismic interpretation in the upper portion of the submarine scar (area shown in Figure 2), the failure surface developed a few meters above seismic reflector R1 in the West depression, whereas the failure developed on R1 in the East depression (Figure 6c). The location of the failure surface of the submarine event was mapped across the landslide scar and the previous topography was estimated according to the location of the lateral flanks. The volume estimate for the submarine scar reaches 1.3 km^3, which implies an average escarpment height of 24 m across the area of the starting zone, which is 54 km^2.

Seismic surveys onshore and offshore allow the definition of seismic characteristics that correlate for the subaerial and submarine portions of the delta area. For the reconstitution of the landslide events, it becomes significant to recognize that seismic unit U3 on the subaerial and submarine profiles consists of low amplitude conformable reflections whereas Unit 4 contains parallel reflections on both onshore and offshore surveys and, on the submarine profiles, contains transparent reflection pattern and truncated reflectors. These observations imply that the sedimentological and geotechnical properties obtained from the coastal borehole (Figure 7) can be used to characterize the properties of the seismic subaerial and submarine units defined elsewhere around the Betsiamites landslide complex.

9. 1663 Colombier landslide failure phases

Various indications suggest that several failures occurred at different times in the Betsiamites River area. In addition to the two early Holocene submarine failures dated as older than 9250 and 7250 cal BP, the integration of the results allows distinguishing that the large Colombier subaerial scar was the result of a complex slide initiated by the 1663 earthquake. In this section, it is demonstrated that the 1663 Colombier landslide event resulted from four related failure phases which all probably occurred one after the other in a short period of time (hours or days). The sequence of events in the triggering and development of the failures is therefore presented.

9.1. Interpretation of initial topography and morpho-stratigraphy

The subaerial and submarine initial morpho-stratigraphy of the Colombier landslide area is interpreted on the basis of the CPTU results, borehole data and seismic profiling (Figure 14). Onshore, the slope of all three delta plains of the marine terraces was likely around 1° (Figure 15a), as it is for the surrounding terrain.

The lithological units involved in the Colombier subaerial landslide fine glaciomarine sediments (U3), stratified paraglacial prodeltaic sediments (U4), and littoral sand (U4-sand) (Figure 14). Sediment thickness increases toward the center of the delta and geotechnical properties of glaciomarine sediments (U3) change according to their elevation above sea-level. The upper sandy layer (U4-sand, 6-L4b) is only 5 m thick (Figure 8) west of the landslide, whereas it is about 25–30 m thick in the East area (see CPTU 46001 in Figure 12). This difference in sand accumulation is a result of the distance from the river; the thickest accumulation being proximal to the river, and had an impact on the type of mass movement developing in the slope. The transition to stratified facies (U4) is at lower elevation in the East zone, at about 5 m closer to the shoreline and potentially up to an

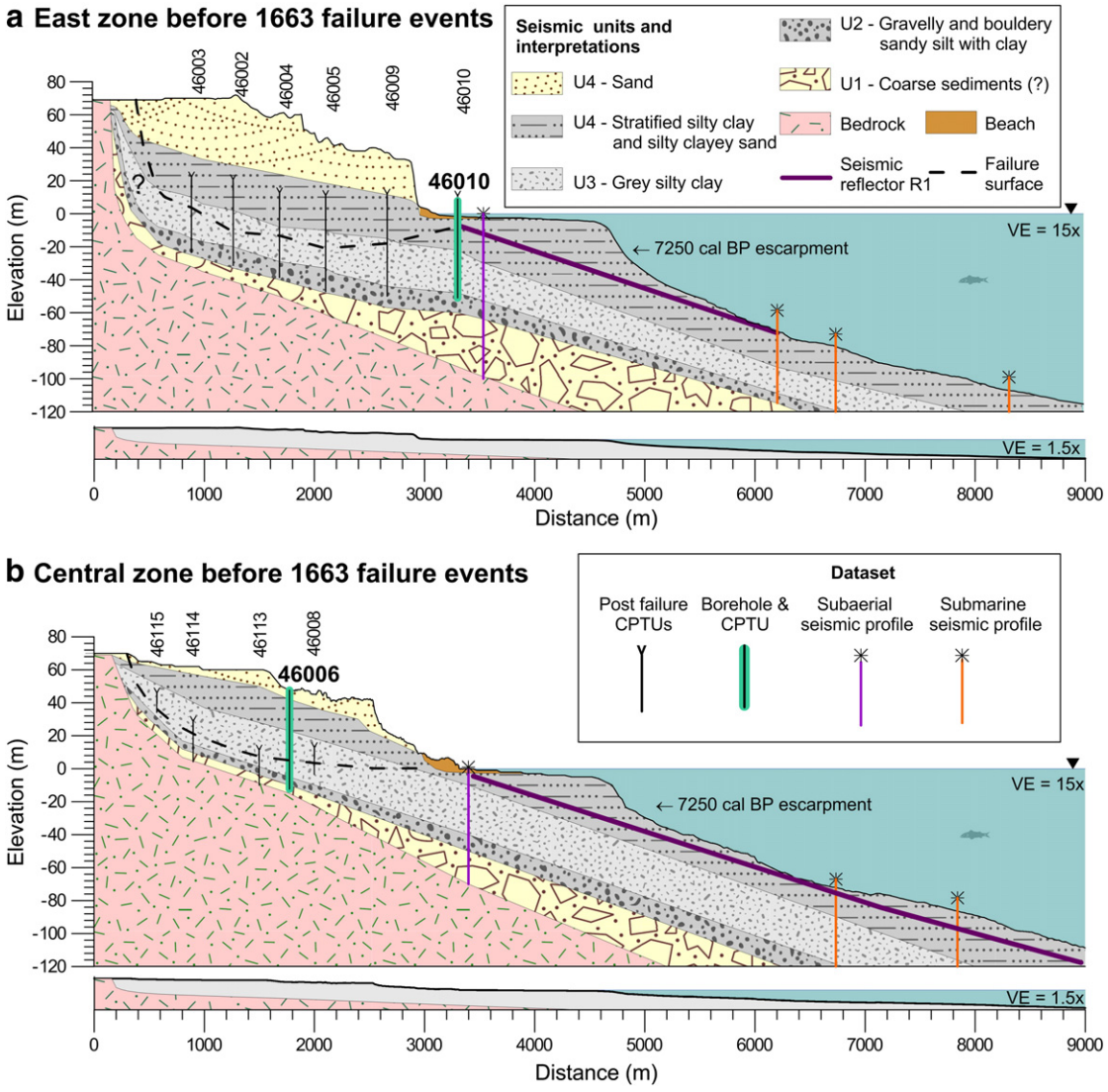

Fig. 14. Lithostratigraphy prior to the 1663 failure phases for the a) East zone and b) Central zone. Lower sections present the topographic profiles at VE = 1.5×. Refer to Fig. 15a for locations of the interpreted profiles.

elevation of 30 m higher upslope. In the Central (Figure 14b) and West zones this transition occurs at higher elevation, as identified at 42 m at site 46006 (Figure 8).

Below sea-level, the same lithostratigraphic units extend seaward (Figure 14). The upper part of the of 8° back scarp of the 7250 cal BP Betsiamites submarine failure (see position in Figure 2) is at an approximate water depth of −10 m. Reflector R1, which appears on the subaerial seismic profile (Figure 6a) and the submarine profiles (Figure 6c) is interpreted as a sandy later (Figure 10). This sandy layer probably came into sight in the lower portion of the back escarpment of the Betsiamites scar (Figure 14a). This sandy layer (R1) also likely extended inland in the unit of stratified silty clay and silty clayey sand (U4, 4-L4) but the Colombier landslide event eroded it making its recognition with CPTU soundings onshore impossible. When reconstructing the topography prior to the 1663 Colombier landslides (Figure 15a), it is interpreted that the location of borehole F46010, now onshore, was a few meters below sea-level (Figure 14a).

9.2. Interpretation of the 1663 Colombier landslide phases

The Colombier subaerial landslide scar (Figure 3) is a complex slide resulting from at least three failure mechanisms: a submarine landslide event, a flowslide in sensitive clay and a lateral spread, as defined by Cruden and Varnes (1996). This landslide scar resulted from 4 distinct failure phases, which all probably occurred one after the other in a short period of time (hours or days). The submarine slide, Phase 1, occurred first. It was followed by a flowslide, Phase 2F in the West Zone, then by a second flowslide, Phase 3F in the Central zone, and finally, likely synchronously, by a spread, Phase 3S, in the East zone (Figure 15b).

9.2.1. Phase 1—submarine failure

Phase 1 occurred first underwater and mobilized part of the beach to an approximate location between the shoreline and the 40 m terrace (Figure 15b). Prior to this submarine failure, the 8° and 20 m high upper escarpment of the 7250 cal BP Betsiamites landslide scar (Figure 5) probably followed the −10 m contour line (Figure 2). Presumably, the 1663 earthquake liquefied a sandy layer, possibly R1 (Figure 10) or a layer similar to it, emerging in the submarine headwall at a water depth of −40 m (Figure 14a). This planar failure probably reached above the current shoreline up to at least the location of soundings C46036, C46010 and C46037 (Figure 10). On those shoreline CPTU soundings, the subaerial landslide debris deposits are interpreted at elevations ranging between −13.5 and

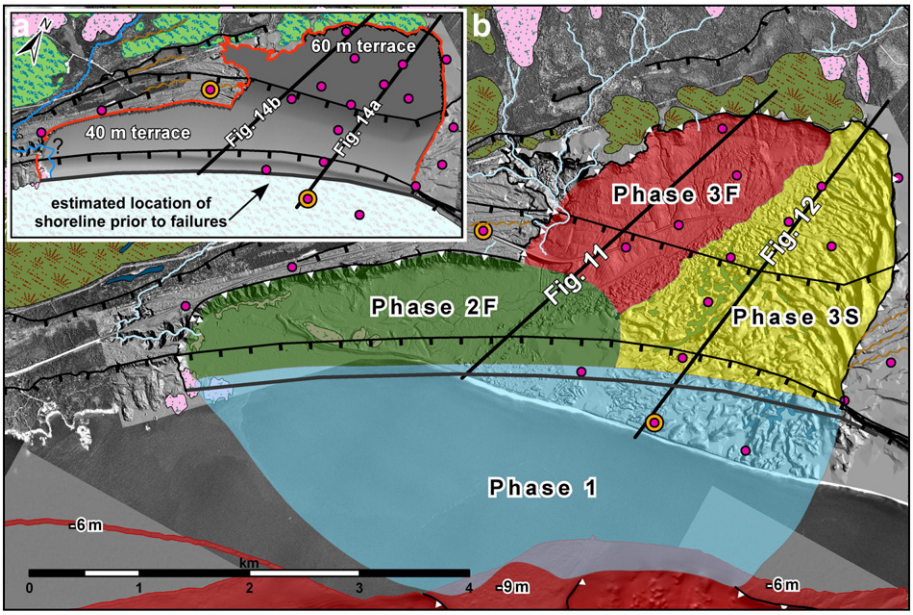

Fig. 15. Initial topography and 1663 failure phases: a) subaerial topography prior to the 1663 complex slide; b) definition of boundaries of 1663 landslide slide phases. See Fig. 2 for legend.

−6 m. Large blocks of deformed and rotated sediment beds (Figure 4) are observable on the beach at low tide. The space below the current shoreline must have been made available for debris spread prior to the subaerial failures, hence supporting the hypothesis of a submarine failure occurring first. More than 145 hm^3 of material were mobilized over an approximate area of 9.3 km^2, which implies an average height of 15.6 m for the submarine landslide body.

It is difficult, on the basis of available data, to define the exact lateral extension of the 1663 Colombier submarine failure (Phase 1). The back escarpment of the 7250 cal BP Betsiamites event in the East depression was eroded (Figure 2) by this submarine failure, which provides an approximate southern boundary. However, the absence of an escarpment on the bathymetric map in the West depression could suggest that: (1) the Colombier submarine failure also occurred on the crest of the Betsiamites submarine scar in the West depression and eroded this escarpment; or (2) the debris of the Colombier subaerial failures simply covers the back escarpment of the Betsiamites submarine scar. The rotated and deformed blocks along the shoreline (Figure 4) extend at least to the proposed boundary of the submarine failure 1 (Figure 15b). As a result, the volume estimation of 145 hm^3 for the submarine slide involves uncertainties.

9.2.2. Phase 2F—west flowslide

Shortly after the submarine failure (Phase 1), it is interpreted that a large subaerial flowslide (Figure 15b) developed in the West zone. The 40 m marine terrace is truncated by the western flank (Figure 3b) of the flowslide. This truncation provides the main evidence to interpret that this area was eroded by a flowslide. The bedrock outcrops on the shoreline (Figure 2) and is estimated around −10 m at site 46006. The presence of bedrock implies that the failure surface could not be much lower than sea-level and thus indicates that it was likely in the unit of laminated silt to silty sand (06-L3a) identified in borehole 46006 (Figure 8). The height of the back escarpment of the landslide is about 45 m, which is similar to the thickness of the landslide body estimated in the Central zone (Figure 11). The liquidity index of the soil in the upper portion of the slope (6-L4a and 6-L3c) is above 1.2 (Table 3), which likely facilitated development of a flowslide (e.g., Leroueil et al., 1996). If it is assumed that the failure surface developed only on land and stopped at the shoreline and that the failure surface was at sea-level, the estimated volume for this phase of the subaerial landslide is about 130 hm^3. The retrogression distance from the interpreted shoreline ranges between 800 and 1200 m. This section of the subaerial scar has an area of 3.4 km^2 and an average width of 3.1 km. Landslide debris appear totally evacuated from the subaerial scar and flowed into the estuary. On the marine seismic profile, the layer of debris related to this event is interpreted to be less than 10 m thick, thus less than 22% of the initial slope height.

9.2.3. Phase 3F—central flowslide

Shortly after the first flowslide (Phase 2F), a second flowslide (Phase 3F) developed in the Central zone. Flowslide 2F acted in fact as an initial failure leaving an unstable backscarp in which flowslide 3F developed. The estimated area for flowslide 3F is 2.5 km^2 and the maximum retrogressive distance was likely between 2600 and 3000 m. The volume of displaced material in this area of the subaerial scar is 75 hm^3. The debris of flowslide 3F moved westward into the open space created by flowslide 2F and into the scars of the submarine failures of 1663 (Phase 1) and 7250 cal BP. Only a 3–4 m thick layer of debris remains in the Central area of the subaerial scar, confirming that this phase is indeed a flowslide (Figure 11). Four CPTUs were carried out in the upper west Central area (Figure 2). Refusal was met at depths between 14.6 and 22.8 m, which is generally shallower than the soundings carried out in the East zone (Figures 12 and 16), suggesting that the bedrock is not as deep in this area.

Few uncertainties remain in regard to the exact position of the failure surface. It appears that the failure surface of flowslide 3F was actually above the shoreline and did not follow the same level as the failure surface of the submarine failure (Phase 1) or the west flowslide 2F. The failure surface of the central flowslide 3F is interpreted to be at an elevation of 7.3 m on CPTU C46008, which was carried out at an elevation of 11.1 m. The location of the failure surface indicates that the 8 m high escarpment left in the western portion of the central scar (Figure 3c) could be in fact the lower part the headwall of the west flowslide 2F and where, subsequently, the failure surface of Phase 3F came into sight. The transition of $I_L > 1$ and $I_L < 1.2$ occurs at about 18 m (Figure 8) at borehole site 46006, 400 m west of the escarpment of Phase 3F and that the failure surface is located at 7.3 m at the position of CPTU 46008. The surface between this transition at borehole 46006 and the failure surface at site 46008 makes an angle of 0.4°. This

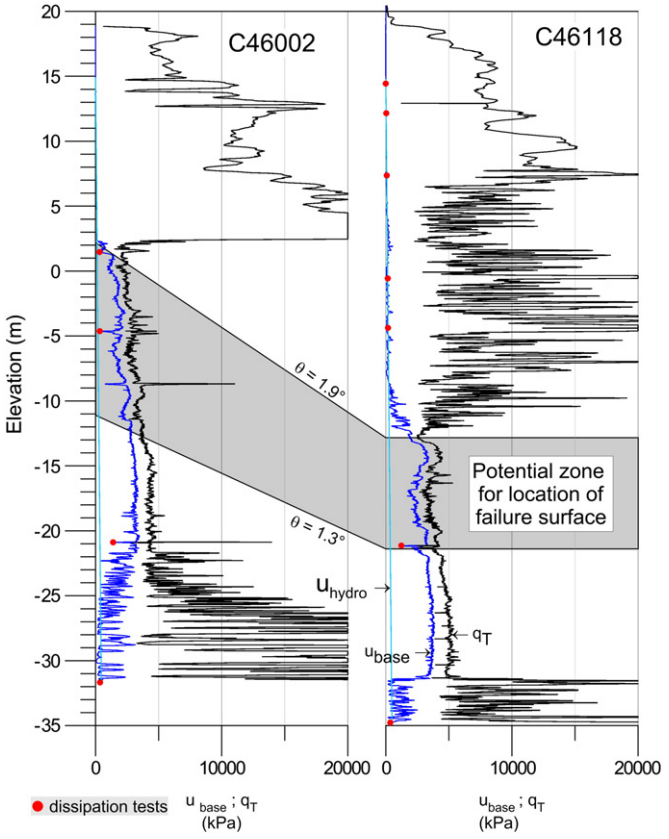

Fig. 16. CPTU 46002 (left graph) and 46118 (right graph) carried out in the East zone. The failure surface is interpreted at a minimum of 2 m and at −13 m, which corresponds to an angle of 1.9° between both soundings.

surface where a significant change in liquidity index occurs could potentially correspond to the plane of retrogression of the failure.

9.2.4. Phase 3S—lateral spread

As a result of the destabilization of the shoreline by the 1663 Colombier submarine failure (Phase 1) and associated flowslides 2F and 3F, Phase 3S occurred (Figure 15b). Flowslide 3F and the lateral spread 3S probably occurred more or less simultaneously but the remolded material of the flowslide 3F evacuated the scar more rapidly and pushed east the sandy and stiffer blocks of spread 3S (green and yellow ridges in Figure 2). The boundary between Phase 3S and 3F is approximate and based on the morphology of the debris remaining in the scar. The debris remaining in the scar of the lateral spread 3S is characterized by a repetitive pattern of ridges and troughs mostly oriented perpendicular to the direction of movement, which is typical of lateral spreads (Cruden and Varnes, 1996). Few blocks of clayey material moved underwater toward the central butte and in the West depression of the 7250 cal BP Betsiamites landslide scar, but most of the blocks are found in the East depression. It is thought that these clayey materials were initially between the failure surface and the sandy layer (U4-sand, 6-L4b) above and were extruded under the weight of the sand layer. The maximum distance between the location of the interpreted location of the back scarp left by the submarine slide (Phase 1) and the back escarpment of the spread (phase 3S) is 2600 m. The approximate width of the landslide body of this phase 3S is about 1300 m. CPTU C46118 (Figure 16) is the only sounding directly in the center of the lateral spread and shows the failure surface to be at least at −13 m (Figure 2). In fact, since the area has a complex lithostratigraphy and there is no core validation, it is difficult to define exactly the position of the failure surface on CPTU 46118 (Figure 16). To account for the uncertainties in the failure surface location, a potential zone for its elevation is indicated. The topographic profile with CPTU results shown in Fig. 12 lies more or less at the boundary between both the flowslide 2F and the spread 3S. The angle of the failure surface between soundings C46118 and C46002 along the section is only 1.9°. As observed for the cross-section along the shoreline, the failure surface likely followed a gently inclined bedding surface. The area of the lateral spread 3S is about 3.7 km^2 and mobilized an estimated slide volume of 180 hm^3.

10. Conclusions

The prediction of landslide activity along the coast of the St. Lawrence estuary and the evaluation of the potential for submarine failures to reach the current shoreline are significant and should be integrated in geohazard mapping and coastal planning. This reconstruction of the sequence of landslide events of the Betsiamites landslide complex demonstrates that the 1663 submarine failure retrogressed upslope and destabilized the subaerial shoreline, which subsequently caused a large multi-component subaerial landslide. In this case, the stability of the slope prior to 1663 failure events was reduced by the presence of the 7250 cal BP Betsiamites submarine scars that acted as a predisposition factor by changing the general geometry of the slope. Mapping of previous shallow submarine scars should hence be integrated in subaerial landslide danger analysis.

In summary, this investigation of the coastal instabilities in the Betsiamites River delta area enabled the identification of a landslide complex of 74 km^2 in the subaerial and submarine domains. The Betsiamites landslide complex was likely formed by at least three landslide events. A first submarine landslide, dated at about 9250 cal BP, which involved at least 200 hm^3 is followed by a second failure, the Betsiamites submarine landslide event dated at 7250 cal BP, which mobilized a volume of 1.3 km^3 over an area of 54 km^2.

The third landslide event is the Colombier landslide initiated by the 1663 earthquake, which involved 4 successive failure phases: one submarine and three subaerial. The Colombier submarine slide (Phase 1) involved a volume of 145 hm^3 over 9.3 km^2 and was likely triggered by the 1663 earthquake. The second phase, flowslide 2F, developed in sensitive material and involved a volume of 130 hm^3 over an area of 3.2 km^2. Phase 3F is a flowslide that occurred in the back headwall of flowslide 2F and mobilized 75 hm^3 over more than 2.5 km^2. Phase 3S is a lateral spread, which extended over 3.8 km^2 with an estimated volume of 180 hm^3. The total volume of material mobilized in 1663 is 530 hm^3 over 20 km^2, which is among the largest documented subaerial landslides in Canada.

Acknowledgments

The authors wish to thank the Ministère des Transports du Québec (MTQ), NSERC and FQRNT for their financial support. We thank the MTQ for the permission to use their topographic and LIDAR surveys, borehole, and piezocone soundings data of the Colombier—Betsiamites area, and in particular to D. Robitaille and P. Locat for their involvement in the project. Many thanks to D. Turmel and C. Amiguet (Université Laval) for their valuable help during seismic reflection data acquisition and to A. Pugin (Geological Survey of Canada, Ottawa) for his assistance with seismic data processing. We recognize the contribution of Patrick Lajeunesse and all scientists and crew members on board the Coriolis II, F.G. Creed, and Guillemot vessels. The Canadian Hydrographic Service and GSC-Quebec are also acknowledged for their contribution to bathymetric data acquisition. Constructive reviews by an anonymous reviewer and M. Geertsema greatly improved the quality of this paper.

References

Adams, J., Atkinson, G., 2003. Development of seismic hazard maps for the proposed 2005 edition of the National Building Code of Canada. Can. J. Civ. Eng. 30, 255–271.

Barletta, F., St-Onge, G., Stoner, J.S., Lajeunesse, P., Locat, J., 2010. A high-resolution Holocene paleomagnetic secular variation and relative paleointensity stack from eastern Canada. Earth Planet. Sci. Lett. 298 (1–2), 162–174.

Bernatchez, P., 2003. Évolution littorale holocène et actuelle des complexes deltaiques de Betsiamites et de Manicouagan-Outardes: synthèse, processus, causes et perspectives. Département de géographie. Université Laval, Québec, p. 460.

Campbell, C., Duchesne, M.J., Bolduc, A., 2008. Geomorphological and geophysical evidence of Holocene instability on the Southern slope of the Lower St. Lawrence Estuary, Québec. In: 4th Canadian Conference on Geohazards : From Causes to Management. Presse de l'Université Laval, Québec, pp. 367–374.

Cauchon-Voyer, G., 2007. Morpho-sédimentologie et mouvements de masse au large de la Rivière Betsiamites, estuaire du Saint-Laurent, Québec. Département de géologie et de génie géologique. Université Laval, Québec, p. 196.

Cauchon-Voyer, G., 2011. Mouvements de masse en milieu côtier dans l'estuaire du Saint-Laurent, Québec, Canada: le cas du grand complexe des glissements de terrain de Betsiamites. Département de géologie et de génie géologique. Université Laval, Québec, p. 374.

Cauchon-Voyer, G., Locat, J., St-Onge, G., 2008. Late-Quaternary morpho-sedimentology and submarine mass movements of the Betsiamites area, Lower St. Lawrence Estuary, Quebec, Canada. Mar. Geol. 251, 233–252.

Christian, H.A., Mosher, D.C., Mulder, T., Barrie, J.V., Courtney, R.C., 1997. Geomorphology and potential slope instability on the Fraser River Delta foreslope, Vancouver, British Columbia. Can. Geotech. J. 34, 432–446.

Cruden, D.M., Varnes, D.J., 1996. Landslide types and processes. In: Turner, A.K., Schuster, R.L. (Eds.), Landslides Investigation and Mitigation. Transportation Research Board, Washington DC, pp. 36–75.

Demers, D., Leroueil, S., 2002. Evaluation of preconsolidation pressure and the overconsolidation ratio from piezocone tests of clay deposits in Quebec. Can. Geotech. J. 39, 174–192.

Dionne, J.C., 1977. La Mer de Goldthwait au Québec. Geogr. Phys. Quat. 16, 61–80.

Dionne, J.C., 2001. Relative sea-level changes in the St. Lawrence estuary from deglaciation to present day. In: Weddle, T.K., Retelle, M.J. (Eds.), Deglacial History and Relative Sea-level Changes, Northern New England and Adjacent Canada. Geological Society of America Special Paper, Boulder, Colorado, pp. 271–284.

Dionne, J.C., Occhietti, S., 1996. Aperçu du Quaternaire à l'embouchure du Saguenay, Québec. Geogr. Phys. Quat. 50, 5–34.

Dredge, L.A., 1976. Quaternary geomorphology of the Quebec North Shore, Godbout to Sept-Iles. , p. 268. University of Waterloo, Waterloo.

Dredge, L.A., 1983. Surficial Geology of the Sept-Îles area. Geological survey of Canada.

Dubois, J.-M.M., 1977. La déglaciation de la Côte-Nord du Saint-Laurent. Geogr. Phys. Quat. 16, 229–246.

Duchesne, M.J., Long, B.F., Urgeles, R., Locat, J., 2003. New evidence of slope instability in the Outardes Bay delta area, Quebec, Canada. Geo-Mar. Lett. 22, 233–242.

Duchesne, M., Pinet, N., Bolduc, A., Bédard, K., Lavoie, D., 2007. Seismic stratigraphy of the lower St Lawrence River estuary (Quebec) Quaternary deposits and seismic signature of the underlying geological domains. Geological Survey of Canada.

Duchesne, M., Pinet, N., Bédard, K., St-Onge, G., Lajeunesse, P., Campbell, D., Bolduc, A., 2010. Role of the bedrock topography in the Quaternary filling of a giant estuarine basin: the Lower St. Lawrence Estuary, Eastern Canada. Basin Research 9999. .

Franconi, A., Sharma, K.N.M., Laurin, A.F., 1975. Région des rivières Betsiamites (Bersimis) et Moisie. Québec; Ministère des richesses naturelles. Direction générale des mines, Service de l'exploration géologique.

Gagné, H., 2008. Géomorphologie et géologie marine du Quaternaire du secteur Trois-Pistoles-Forestville, estuaire du Saint-Laurent (Québec). Département de géographie. Université Laval, Québec, p. 89.

Hart, B.S., Long, B.F., 1996. Forced regressions and lowstand deltas: Holocene Canadian examples. J. Sediment. Res. 66, 820–829.

Hillaire-Marcel, C., Causse, C., 1989. Chronologie Th/U des concrétions calcaires des varves du lac glaciaire de Deschaillons (Wisconsinien inférieur). Can. J. Earth Sci. 26, 1041–1052.

Josenhans, H., Lehman, S., 1999. Late glacial stratigraphy and history of the Gulf of St. Lawrence, Canada. Can. J. Earth Sci. 36, 1327–1345.

Lajeunesse, P., St-Onge, G., Locat, J., Labbé, G., 2007. Multibeam bathymetry and morphostratigraphy of submarine gravity flows and slopes failures in the St. Lawrence Gulf and Lower Estuary (Québec, Canada). In: Lykousis, V., Sakellariou, D., Locat, J. (Eds.), Submarine Mass Movements and Their Consequences. Springer, p. 27.

Lamontagne, M., Keating, P., Perreault, S., 2003. Seismotectonic characteristics of the Lower St. Lawrence Seismic Zone, Quebec: insights from geology, magnetics, gravity, and seismics. Can. J. Earth Sci. 40, 317–336.

Lamontagne, M., Halchuk, S., Cassidy, J., Rogers, G., 2008. Significant Canadian earthquakes of the period 1600–2006. Seismol. Res. Lett. 79, 211.

Lasalle, P., Chagnon, J.-Y., 1968. An ancient landslide along the Saguenay River, Quebec. Can. J. Earth Sci. 5, 548–549.

Leroueil, S., Tavenas, F., Le Bihan, J.-P., 1983. Propriétés caractéristiques des argiles de l'est du Canada. Can. Geotech. J. 20, 681–705.

Leroueil, S., Vaunat, J., Locat, J., Picarelli, L., Lee, H., Faure, R., 1996. Geotechnical characterization of slope movements. In: Senneset, K. (Ed.), 7th International Symposium on Landslides, Trondheim, pp. 53–74.

Locat, J., in press. La localisation et la magnitude du séisme du 5 février 1663 (Charlevoix) revues à l'aide des mouvements de terrain. Can. Geotech. J.

Locat, J., Tanaka, H., Tan, T.S., Dasari, G.R., Lee, H., 2003. Natural soils: geotechnical behaviour and geological knowledge. In: Tan, T.S., Phoon, K.K., Hight, D.W., Leroueil, S. (Eds.), Characterisation & Engineering Properties of Natural Soils, 1, pp. 3–28.

Locat, J., Amiguet, C., Cauchon-Voyer, G., Bolduc, A., Demers, D., Mosher, D., Sanfaçon, R., Godin, A., Lajeunesse, P., St-Onge, G., 2008. Instabilités sous-marines et côtières le long de la rive nord du Saint-Laurent, entre Pointe-des-Monts et Saint-Siméon: analyse préliminaire, Quebec 2008: 400 Years of Discoveries. Joint Meeting of the Geological Association of Canada, Mineralogical Association of Canada, Society of Economic Geologists and the Society for Geology Applied to Mineral Deposits. Revue des résumés, Québec, p. 99.

Lunne, T., Robertson, P.K., Powell, J.J.M., 1997. Cone Penetration Testing in Geotechnical Practice. Blackie Academic—Chapman-Hall Publishers.

Massé, M., 2001. Évolution générale des dépôts quaternaires sous l'estuaire du St-Laurent entre l'Îles aux Lièvres et Rimouski. Université du Québec à Rimouski, Rimouski, p. 129.

Massé, M., Long, B., 2001. Slope instability seismic signatures in Quaternary sediments of the St. Lawrence estuary, Proceedings of 2001 An Earth Odyssey, International Association of Hydrogeologists. The Canadian Geotechnical Society, pp. 784–791.

McKenna, G.T., Luternauer, J.L., Kostaschuk, R.A., 1992. Large-scale mass-wasting events on the Fraser River Delta front near sand heads, British Columbia. Can. Geotech. J. 29, 151–156.

Mosher, D.C., 2008. Submarine mass movements: geohazards with far-reaching implications. In: Locat, J., Perret, D., Turmel, D., Demers, D., Leroueil, S. (Eds.), 4e Conférence canadienne sur les géorisques: des causes à la gestion - 4th Canadian Conference on Geohazards : From Causes to Management. Presse de l'Université Laval, Québec, pp. 55–62.

Mulder, T., Alexander, J., 2001. The physical character of subaqueous sedimentary density flows and their deposits. Sedimentology 48, 269–299.

Piper, D.J.W., Hiscott, R.N., Normark, W.R., 1999. Outcrop-scale acoustic facies analysis and latest Quaternary development of Hueneme and Dume submarine fans, offshore California. Sedimentology 46, 47–78.

Potvin, J., Pellerin, F., Demers, D., Robitaille, D., La Rochelle, P., Chagnon, J.-Y., 2001. Revue et investigation complementaire du site du glissement de Saint-Jean-Vianney. 54th Canadian Geotechnical Conference, pp. 792–800.

Pullan, S.E., MacAulay, H.A., 1987. An in-hole shotgun source for engineering seismic surveys. Geophysics 52, 985–996.

Robertson, P.K., 1990. Soil classification using the cone penetration test Canadian. Geotechnical J. 27, 151–158.

Smith, W., 1962. Earthquakes of Eastern Canada and Adjacent Areas, 1534–1927. Publications of the Dominion Observatory, Ottawa. pp. 271–301.

St-Onge, G., Stoner, J.S., Hillaire-Marcel, C., 2003. Holocene paleomagnetic records from the St. Lawrence Estuary, eastern Canada: centennial- to millennial-scale geomagnetic modulation of cosmogenic isotopes. Earth Planet. Sci. Lett. 209, 113–130.

St-Onge, G., Lajeunesse, P., Duchesne, M., Gagné, H., 2008. Identification and dating of a key Late Pleistocene stratigraphic unit in the St. Lawrence Estuary and Gulf (Eastern Canada). Quaternary Sci. Rev. 27, 2390–2400.

Stuiver, M., Reimer, P., 1993. Extended ^{14}C database and revised CALIB radiocarbon calibration program. Radiocarbon 35, 215–230.

Sultan, N., Cochonat, P., Canals, M., Cattaneo, A., Dennielou, B., Haflidason, H., Laberg, J.S., Long, D., Mienert, J., Trincardi, F., Urgeles, R., Vorren, T.O., Wilson, C., 2004. Triggering mechanisms of slope instability processes and sediment failures on continental margins: a geotechnical approach. Mar. Geol. 213, 291–321.

Syvitski, J.P.M., Praeg, D., 1989. Quaternary Sedimentation in the St. Lawrence Estuary and adjoining areas, Eastern Canada : an overview based on high resolution seismo-stratigraphy. Geogr. Phys. Quat. 43, 291–310.

Thwaites, R.G., 1959. The Jesuit Relations and Allied Documents: Travels and Explorations of the Jesuit Missionaries in New France, 1610–1791: The Original French, Latin, and Italian texts, with English Translations and Notes. Pageant Book Co, New York.